FH JOANNEUM

Master Thesis

Permittivity Measurement

Concept Proof of the Denoth Meter

Author: Stefan Dierer

Supervisor: FH-Prof. Dipl.-Ing. Dr. techn Robert Okorn

Advanced Electronic Engineering

4.12.2017

V1.05

Declaration

I hereby declare that the present master thesis was composed by myself and that the work contained herein is my own. I also confirm that I have only used the specified resources. All formulations and concepts are taken verbatim or in substance from printed or unprinted material or from the Internet have been cited according to the rules of good scientific practice and indicated by exact references to the original source.

The present thesis has not been submitted to another university for the award of an academic degree in this form. This thesis has been submitted in printed and electronic form. I hereby confirm that the content of the digital version is the same as in the printed version.

I understand that the provision of incorrect information may have legal consequences.

_____ Kapfenberg, 4.12.2017

Abstract

This master thesis covers the operating principle of the Denoth meter. The measurement principle and the key figures which are published in the original paper are evaluated with a series of Spice simulations and experiments in the laboratory. An alternative computation method is discussed additionally. Prototype circuits are fabricated for both, the flat-plate sensor and the sensor electronics. An MSP430 microcontroller is considered to provide the source signal and to detect the output signal at an operating frequency of 20MHz. The relative permittivity is a complex quantity where both, the real and the imaginary part need to be determined accurately to achieve reliable results.

Acknowledgements

I would like to express my very great appreciation to Professor Okorn for his valuable and constructive suggestions during the planning and development of this work. His willingness to give his time so generously has been very much appreciated. I would also like to thank the staff of the Advanced Electronic Engineering department for enabling me to visit their offices and for their help in offering me the resources in running the project.

I am particularly grateful for the assistance given by my colleague Christoph Brunnhofer and for all the enlightening discussions we had throughout the years of our studies. I want to thank my friends Marco, Jenny and Mike for the continuous motivation.

Finally, I want to thank my parents and my grandparents who provided the basis for me to accomplish an academic education.

Table of Contents

1. Introduction and Research

1.1. Motivation

Ever since it has been a major challenge to measure the properties of a snowpack to determine its nature in terms of consistency, texture, wetness, density and other quality factors. Especially in Alpine areas, residents depend on reliable avalanche forecasts and efficient artificial snow generation plants. Both can be application fields for a device which measures one of those variables as mentioned above.

1.2. Electromagnetic Properties of Alpine Snow

Snow is a heterogeneous dielectric material which consists of ice, air and liquid water. The dielectric constant of a material that consists of distributed, assumed to be ellipsoidal solid particles and empty holes is defined by volume fractions of these components and their distribution and is depending on frequency and temperature [1].

The dielectric constant is a complex quantity

$$\varepsilon_R(\omega) = \varepsilon_R'(\omega) - j\varepsilon_R''(\omega) \tag{1.1}$$

that decreases monotonically with increasing frequency, but it remains constant in the high frequency domain from 10MHz up to 1GHz. Here, the measurement is controlled primarily by the density and the water content.

The dissipation factor is

$$\tan\delta = \frac{\varepsilon_R''}{\varepsilon_R'} \tag{1.2}$$

given by the ratio between the polarization losses ε_R'' which is because of friction between the dipole moments and the relative permittivity ε_R' of the dielectric material.

A simple quadratic equation was discovered empirically by A. Denoth and others [2]. It describes the relation between the relative permittivity, the water content (in %) and the density of snow (in gm^{-3}) for wet and dry snow, respectively:

$$\varepsilon_R' = 1 + 1{,}92\rho + 0{,}44\rho^2 + 0{,}187W + 0{,}005W^2 \tag{1.3}$$

$$\varepsilon_R' = 1 + 0{,}851\rho^2 \tag{1.4}$$

To measure the density/wetness of snow with an electronic device, a tradeoff must be made: either the water equivalent is measured separately (e.g. with a freezing calorimeter) or a quadratic equation is used which can only be applied for dry snow where the water content is negligibly small (equation 1.4). The Denoth meter was invented to perform long-term snow wetness recording where the snow density was measured separately (equation 1.3). A gravimetric determination with a cylinder and a spring balance is a destructive measurement and therefore, it is desirable to be avoided.

If the water content is high, polarization losses are high too. Liquid water at 0°C has a relative permittivity of $\varepsilon_R' = 88 - j9.8$, decreasing with increasing temperature [3]. Ice has a relative permittivity of $\varepsilon_R' = 3{,}2 - j0.001$, for air, it is $\varepsilon_R' = 1$. This implies that the relative permittivity of snow is substantially depending on the water content. The imaginary part can only be ignored if the snow is dry [4].

Table 1.1: Relative permittivity of different (snow) samples

Dielectric Material	**Relative Permittivity ε'**	**Comment**
Water	80,1	T=20°C
Ice	3,2	f>100kHz
Air	1,0006	
Fresh snow	1,1	ρ=100 kgm^{-3}, W=0%
Wet snow	3,13	ρ=500 kgm^{-3}, W=5%
Very wet snow	5,0	ρ=750 kgm^{-3}, W=10%
Compact snow	1,6 - 2	[4]

The incremental permittivity $\Delta\varepsilon'$ shows a relation between permittivity and the water content [2]:

$$\Delta\varepsilon' = 0{,}206W + 0{,}0046W^2 \tag{1.5}$$

$$\Delta\varepsilon' = \varepsilon_R' - 1 - 1{,}76(1-\phi) - 0{,}37(1-\phi)^2$$

$$\phi = 1 - \frac{\rho_{snow} - \rho_{water} \cdot W}{\rho_{ice}}$$

with ε_R' according to equation 1.3.

At comparably low frequencies (~20MHz), losses are determined by the water content and snow porosity ϕ, thus ε_R'' cannot be used for the determination of W because effects of ionic conductivity cannot be neglected. Only in the microwave regime (X-band), the influence of snow porosity can be neglected. The grain size of the ice particles is not effective either in the low or in the high frequency domain [1].

1.3. Concept Proof of the Denoth Meter

In 1994, A. Denoth has reported that a promising method to measure the dielectric function of snow at a frequency of 20MHz. A system has been developed which consists of a tuning and display unit and up to four sensor units connected with cables. Sensor tuning and data storage are performed by a low-power microcontroller.

The tuning unit is a handheld device that consists in principal of a microcontroller with an ADC and two DACs for signal conversion, a multiplexer to be able to connect multiple sensors, an LCD display, an EEPROM and a RAM for data, a V24 interface to connect the device to a PC, a real-time clock unit and the minimum detection unit which is supposed to be simple a rectifier.

The sensor unit is an interesting system which consists of a capacitive sensor, an analog circuit (twin-T-bridge) that operates at 20MHz and an analog mixer to down convert the output signal to the kHz-range (both with a separate crystal oscillator). Capacitive tuning and calibration of the bridge is achieved by voltage-controlled varactor diodes. This will be discussed very much in detail in the following sections of this thesis.

The sensor is developed over years in different stages whereby a flat-plate capacitive unit is the most promising implementation for non-destructive, precise and sensitive measurements of the complex relative permittivity. The determination of the real part is accomplished with good accuracy (relative error $E(\varepsilon_R') \cong 2\%$). The imaginary part (ε_R'') is accepted is with reduced accuracy because effects of ionic conductivity are neglected [5].

The measurement is based on the deviation of the capacitance when the sensor is exposed to a specific material compared to a reference measurement.

$$\varepsilon_R = \frac{C_X}{C_0} \tag{1.6}$$

The main task of this thesis is to evaluate the functionality of the flat-plate Denoth sensor and the sensor circuit. The most challenging task is decidedly to obtain the imaginary part of the relative permittivity. One idea is to measure voltage and current at the capacitance to obtain the dissipation factor (equations 1.3 and 1.7). The problem with this method is that the values for the loss angle is very small and in practice very difficult to measure with sufficient accuracy.

$$Z_C = \frac{U}{I} = \frac{1}{j\omega C} \quad \Rightarrow \quad \delta \neq 90° \tag{1.7}$$

The sensor circuit of the Denoth meter is based on a different method to obtain ε_R. The measurement is based on a resonant circuit of a band stop filter. The change of the sensor capacitance causes a deviation of the output frequency and amplitude of the resonance peak. These parameter changes can be compensated with tunable varactor diodes. Reference measurements and calibration of the sensor is necessary to compare corresponding DC voltages at the diodes to determine the complex relative permittivity at a certain measurement frequency. This process is discussed very much in detail with the help of Spice simulation and measurements in the laboratory.

2. Capacitive Sensor

The sensor of the measurement device is a capacitive sensor with a certain shape. Professor Denoth examined and tested volume and surface sensitive sensors of different sizes. Diverse patterns of electrodes, such as comb-shaped, u-shaped or ring-shaped, have led them to the conclusion that the spatial resolution of the sensor depends on its geometric properties. Several sensors have been considered for different operation modes, such as half-space and full-space mode to measure either the dielectric constant of a surface or of a volume. The final version is a flat-plate sensor because it enables a nearly non-destructive measurement with a spatial resolution of 1 to 3 cm depending on the operation mode [2].

For the current project, the sensor shape is reconstructed from a photograph of the original paper. Some geometric dimensions are taken over and some are estimations.

First home-made prototype of a Denoth sensor:

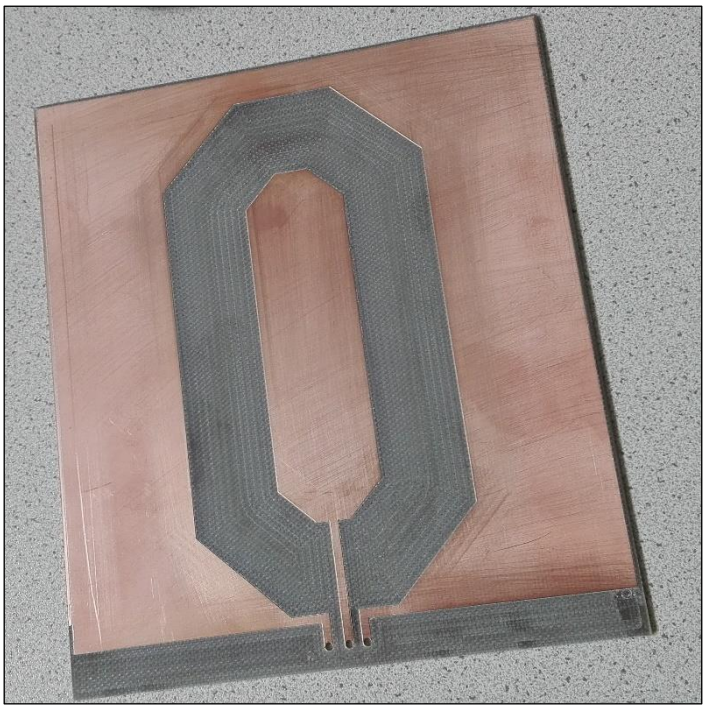

Figure 1.1: Denoth sensor (replica)

The sensor in the picture was fabricated with a copy milling machine according to the estimated dimensions of the original. The PCB is 1.6mm thick, the dielectric material is FR4 and a double-sided copper layer of 350µm. The geometry with the precise dimensions are plotted in appendix A.1. A later version of the sensor is produced with a 3.2mm PCB to reduce parasitic effects of the sensor capacitance of the backplane.

The applicable property of the sensor is its capacitance which is the capacitive element of a tunable parallel resonant circuit.

2.1. Principle of Operation

The resonant frequency of the circuit changes as the values of the inductance or of the capacitance change. The inductor has a fixed value, hence the inductance cannot be influenced.

Denoth sensors consist of shaped electrodes which are considered as two coplanar conducting stripes. It can be mathematically treated as two-dimensional analogon of a plate condenser [2].

The capacitance is proportional to the relative permittivity which is denoted in the nominator, and it depends on the area of the electrodes and their distance to each other. It is granted that solving the equation for coplanar conducting stripes is not as trivial as for a plate condenser, but in fact it may not be necessary. The capacitance is determined empirically with an LCR impedance analyzer with the prototype in the laboratory.

Impedance measurement result:

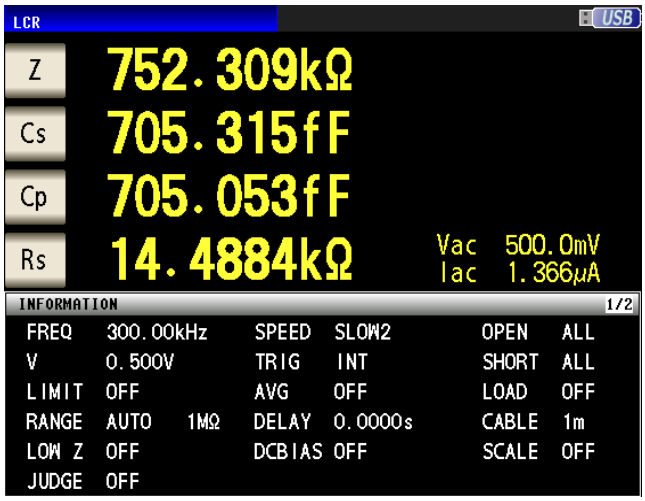

Figure 2.2: Measurement of the sensor impedance

The sensor is operated at a frequency of 20MHz. The capacitance is measured from 100kHz to 5MHz with respect to the limits of the analyzer. The capacitance is given by the geometry of the electrodes and is estimated to remain unchanged until the GHz-range where coupling effects must be considered. The measurement at a lower frequency is estimated to be reasonable. The backplane of the sensor must be bypassed, because the differential capacitance between the electrodes is of interest. Therefore, it is connected to the guard input of the impedance analyzer. If it is not connected to the guard, the capacitances between each electrode and the back plane are measured as a serial capacitance parallel to the differential capacitance.

Different sensor impedance measurement results are plotted in the appendix A.2.

The Capacitance between the outer electrode and the back plane is $C_X = 124{,}6pF$.

The Capacitance between the inner electrode and the back plane is $C_Y = 33{,}6pF$.

The sensor capacitance with a floating backplane is $C_S = 21pF$.

$$C_S = C_{differential} + \frac{1}{\frac{1}{C_X} + \frac{1}{C_Y}} \approx 27pF \tag{2.1}$$

The deviation of the sensor capacitance by 6pF indicates that the differential capacitance increases dramatically if the backplane is connected.

The analyzer must be calibrated right before each recording. Rearrangements after calibration must be avoided. Different measurement configurations have been set up but, unfortunately, with divergent results due to the high sensitivity of the sensor. The capacitance has been observed in a range between 600fF and 1pF depending on the test environment and the analyzer configuration.

Analyzer settings:

- Frequency: 300kHz
- Voltage: 500mV
- Mode: High Z
- Range: Auto (1MΩ)
- Measurement speed: SLOW2
- Cable length: 1m
- Temperature: 23°C

The measurement accuracy is calculated from the basic accuracy which is based on the accuracy of the impedance, the phase angle and the following coefficients:

- C: level coefficient
- D: measurement speed coefficient
- E: cable length coefficient
- F: DC bias coefficient
- G: temperature coefficient

$$Measurement\ Accuracy = Basic\ Accuracy \cdot C \cdot D \cdot E \cdot F \cdot G \tag{2.2}$$

The basic accuracy depends on the measurement range and the impedance of the test sample. The required formulas and a table to obtain the coefficients A and B are given in the instruction manual of the analyzer:

$$Basic\ Accuracy = \left(A \cdot B \cdot \left| \frac{10 \cdot \frac{1}{\omega C}}{Range\ in\ \Omega} - 1 \right| \right) = 1{,}0158\ \% \tag{2.3}$$

The level coefficient is

$$C = 1 + \frac{0{,}3}{V} = 1 + \frac{0{,}3}{0{,}5} = 1{,}6 \tag{2.4}$$

The measurement speed coefficient $D = 1$ is because of the *SLOW2*-configuration.

The cable length coefficient $E = 1{,}5$ is because of the 1m cable plus terminals.

The DC bias coefficient $F = 1$ because the DC bias setting is off.

The temperature coefficient $G = 1$ because the ambient temperature was between 18°C and 28°C.

The measurement accuracy for the impedance equals the measurement accuracy for the phase angle.

$$Measurement\ Accuracy = 1{,}0158 \cdot 1{,}6 \cdot 1{,}5 = 2{,}4379\ \% \tag{2.5}$$

The measurement result of figure 2.2 with $C_{Sensor} = 705fF$ may deviate by $\pm 17{,}2fF$.

The sensor is modeled with a Sonnet Software simulation to confirm this result.

Sonnet Software simulation editor:

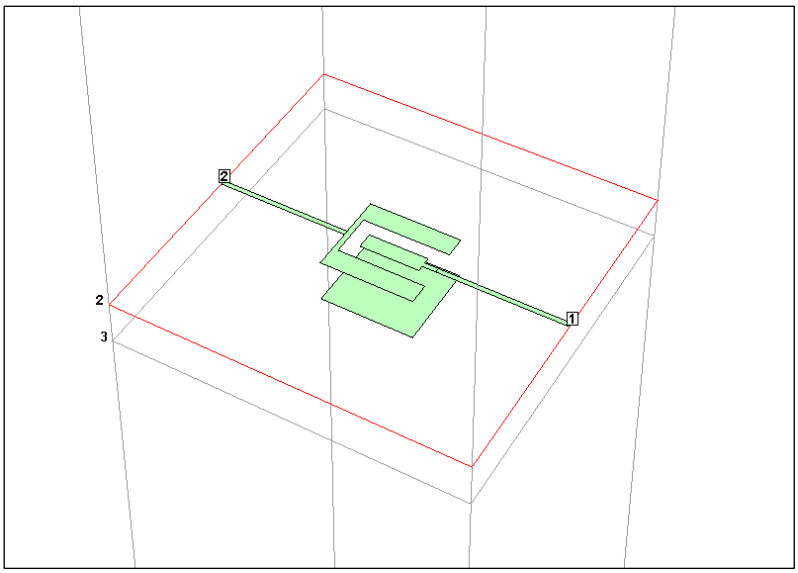

Figure 2.3: Simulation of the electrodes and the backplane

Simulation result:

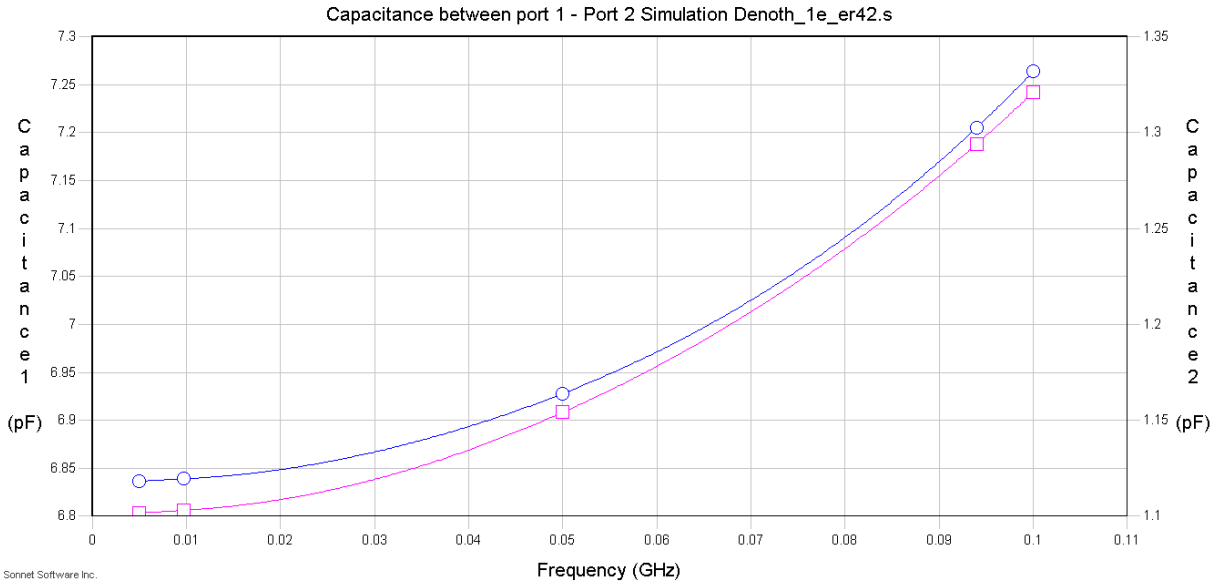

Figure 2.4: Sensor capacitance simulation

Figure 2.3 shows the geometry that is simulated. Figure 2.4 confirms the capacitance measurement of the sensor electrodes and the backplane. The pink curve shows the differential measurement between the electrodes. In contrast to previous expectations is the capacitance depending on frequency, hence a measurement in the kHz-range not sufficient. The blue curve corresponds to the single-ended measurement where the influence of the backplane is obvious. At 20MHz, the differential capacitance is $C_S = 1{,}12pF$, the single-ended measurement yields $C_S = 6{,}85pF$. These results match with those of equation 2.1).

2.2. Resonant Notch

The resonant circuit is part of a higher order band stop filter, henceforth referred to as notch. The original twin-T-brigde of the Denoth meter is taken over, its transfer function calculated, analyzed and finally simulated with OrCAD Capture to evaluate and reuse its operation principle.

Original schematic [5]:

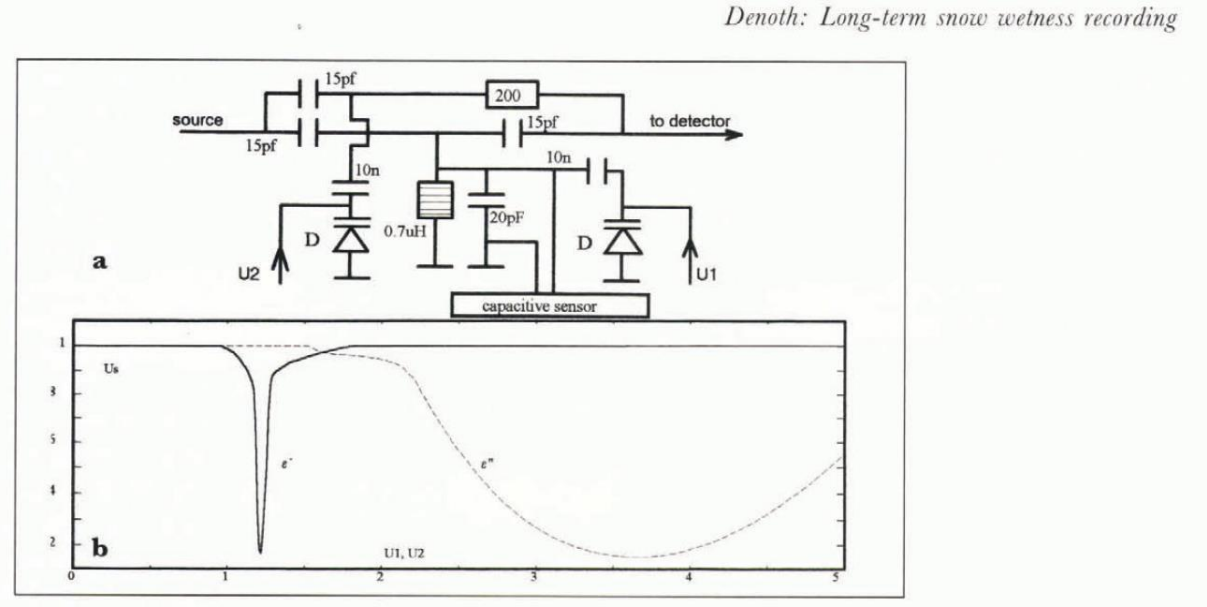

Figure 2.5: Notch filter with resonant circuit

Basically, the circuit consists of a high pass structure which is obviously observable at the input capacitances where lower frequency components are attenuated, and DC components are rejected. Both T-branches of the structure have a special function. A varactor diode in each T-branch enables the tuning process of the circuit which is necessary to obtain both, the real and imaginary part of the complex relative permittivity.

The circuit has been optimized to measure the dielectric constant ε_R of Alpine snow, whereby measuring the real part $\varepsilon_R^{'}$ has a good level of precision. Measuring the imaginary part $\varepsilon_R^{''}$ is only possible with reduced accuracy which must be accepted to a certain extend [5]. The latter corresponds to energy losses in the dielectric material under AC conditions and must be compensated. The circuit is sourced with a 20MHz-signal, thus losses cannot be neglected.

The capacitance of the sensor changes when the permittivity changes. Consequently, the resonant frequency drifts to a lower value that must be compensated by tuning operations. The resonator is part of the notch that's why the value to be detected is a minimum voltage.

2.3. Tuning Diode

Varactor diodes are generally used for oscillator circuits and HF applications to tune a certain frequency. The principle is based on reverse implementation to take advantage of the variable capacitance at the edges of the space charge region around the p-n junction of the diode.

For the current project, the varactor diode requirements are:

- Linear output curve for log(V_R) up to $V_R = 5V$
- low series resistance and low series inductance
- low temperature drift
- operation at subzero temperatures must be guaranteed
- a reasonable capacitance ratio

The diodes that are implemented in the prototype hardware and used for the simulations are BB535 silicon tuning diodes from Infineon. To guarantee a linear behavior for the tuning process, the diodes must show logarithmic behavior in a range from 1V to 5V. The first approach to guarantee the functionality as expected is to check the datasheet of the diode. The characteristic output and temperature curves are of interest.

Output characteristics of BB535:

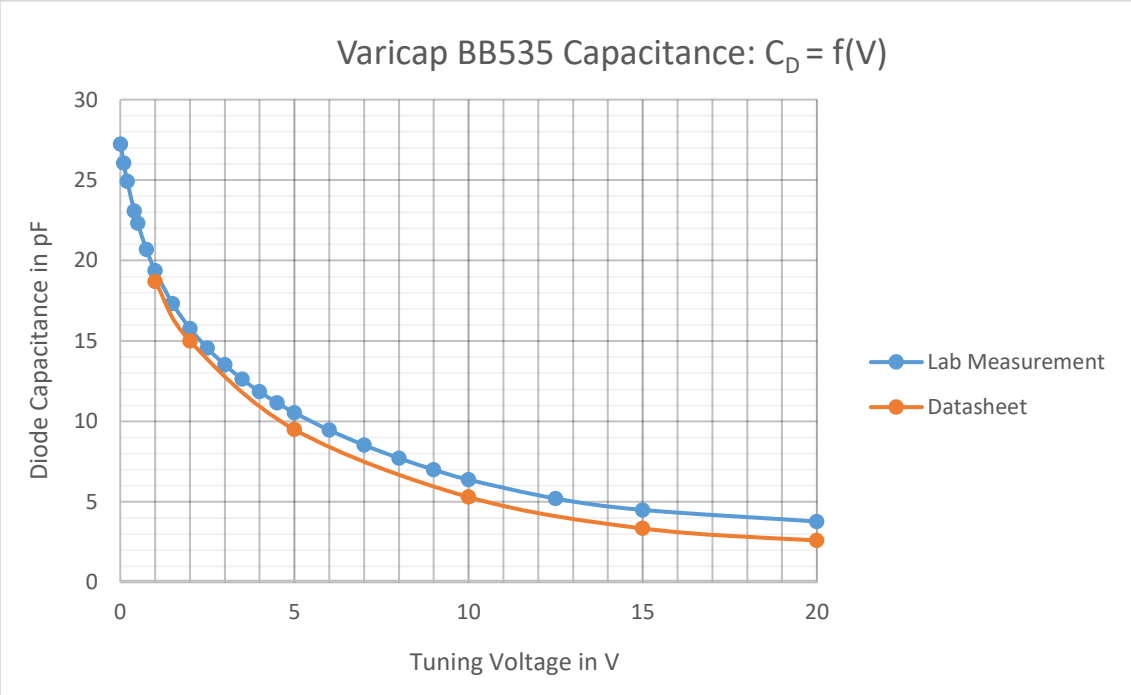

Figure 2.6: Diode capacitance of BB535

The values to draw the diagram in figure 2.6 are extracted from the datasheet and measured in the lab. The nominal output behavior of the diode is assumed to be linear in case of a logarithmic x-axis for a certain voltage range (figure 2.7).

The temperature behavior of the diode, compared to alternative ones with the same or similar behavior, is good. The temperature drift at a reverse voltage $V_R = 1V$ is less than 1% in range between room temperature and its minimum. The absolute temperature range of the component is less satisfying, since a device such as a Denoth meter must function properly at temperatures below -20°C.

The capacitance is ratio is given with 8,9 for a range between 1V and 28V which is the maximum voltage that can be applied to the diode without destroying it. For the current project this is not interesting because the maximum voltage that can be applied by the microcontroller will be 2,5V which is the reference voltage of the DAC. It is planned to use a non-inverting amplifier circuit to reach a tuning voltage with a maximum of 5V.

If the capacitance of the sensor is estimated to change by the factor 5 for very wet snow as an extreme example. The tuning diode needs to operate in a similar range, to tune the output frequency and amplitude back to the minimum. The sensor is estimated to have a capacitance value of typically 1pF. The BB535 diode can be tuned by 9,2pF which would be enough, also for a worse case with a sensor of a higher capacitance.

The series inductance and the series resistance of the diode are very small. The reverse current is very small, typically less than $I_R = 10nA$ for the highest applicable reverse voltage $V_R = 30V$.

Characteristic curve of BB535 with logarithmic x-axis:

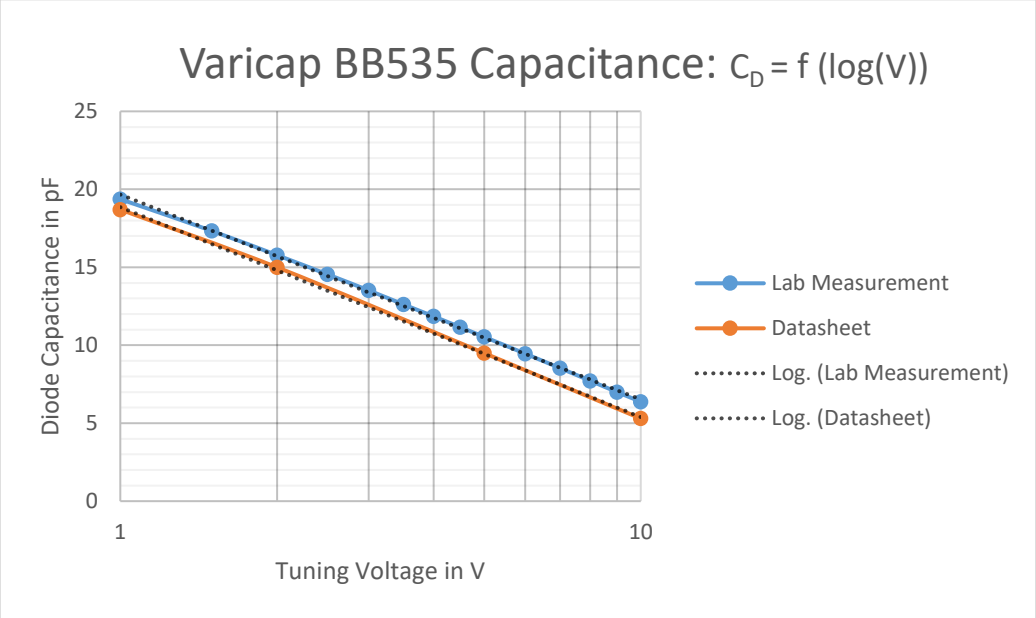

Figure 2.7: Output curve of BB535 (logarithmic scale)

The deviation from the ideal logarithmic behavior is very small (dotted line) for a range between 1V and 10V. The measurement tables to figures 2.6 and 2.7 are given in appendix B4.

2.4. Measurement Principle

The lower T-branch mainly consists of a tunable resonant circuit which is composed of:

- Series resistance of the coil
- Inductance of the coil
- Capacitances of the sensor electrodes, the backplane and the varactor diode

The circuit is arranged to determine the relative permittivity $\varepsilon_R^{'}$ of a material by tuning the varactor diode D_1 in the lower branch and applying equation 2.14.

The sensor must be calibrated with a reference material (air). If a certain output voltage level is reached, the tuning voltage V_{D1} must be denoted as V_{REF}. Now, the sensor must be exposed to the material to be measured. The capacitance of the sensor changes proportional to the change of the relative permittivity. First, losses must be compensated by changing V_{D2}. Secondly, the measured voltage V_M at the varactor diode D_1 must be remembered and transferred to the equation. For calibration it is necessary to cool the sensor down to 0°C (±5°C) so that the temperature coefficient of V_{REF} is negligibly small (≤-0,2%K^{-1}) [5].

The upper branch of the T-bridge is to compensate polarization losses $\varepsilon_R^{''}$. Because of a lossy dielectric material, the output voltage changes in amplitude and slightly in frequency. The amplitude of the output voltage can be affected by tuning the DC voltage at the varactor diode D_2. With this method, those effects can be compensated to a certain extent with a limited degree of accuracy. Simulation measurements will give further information on this topic (section 3.2).

The following equations explain the principle of the measurement that was originally published by A. Denoth in 1994. As already mentioned, the sensor capacitance can be treated as an analogon of a plate condenser, and the dielectric constant is a complex quantity.

$$C = \varepsilon \cdot \frac{A}{d} = (\varepsilon_R' - j\varepsilon_R'') \cdot \varepsilon_0 \cdot k_1 \tag{2.6}$$

The constant k_1 is sensor specific to consider the influence of its structure on the measurement. The reactance of the sensor is:

$$X_C = \frac{1}{j\omega(\varepsilon_R' - j\varepsilon_R'') \cdot \varepsilon_0 \cdot k_1} = \frac{1}{j\omega\varepsilon_0\varepsilon_R' k_1 + \varepsilon_0\varepsilon_R''\omega k_1} \tag{2.7}$$

The admittance is most qualified to separate the susceptance and the conductance:

$$Y_C = j\omega\varepsilon_0\varepsilon_R' k_1 + \varepsilon_0\varepsilon_R'' \omega k_1 \tag{2.8}$$

For a deviation of the capacitance and the relative permittivity, it is correct to say

$$\Delta C = \Delta\varepsilon = C_X - C_0 \tag{2.9}$$

$$\Delta C = (\varepsilon_R' - j\varepsilon_R'')\varepsilon_0 k_1 - \varepsilon_0 k_1 = (\varepsilon_R' - j\varepsilon_R'')k_2 - k_2 \tag{2.10}$$

$$with\ k_1 = \frac{C_S}{\varepsilon_0} \quad \rightarrow \quad k_2 = C_S$$

According to figure 2.7 one may assume to express the capacitance of the diode as a straight line depending on the logarithm of the voltage.

$$C = a_1 - a_2 \cdot \log(V) \tag{2.11}$$

For a deviation of the capacitance we get

$$\Delta C = a_1 - a_2 \cdot \log(V_1) - a_1 + a_2 \cdot \log(V_2) \tag{2.12}$$

$$k_2(\varepsilon_R' \neq 1):\ \Delta C = a_2 \cdot \log\left(\frac{V_2}{V_1}\right) \tag{2.13}$$

This calculation enables the determination of the relative permittivity by the formula

$$\varepsilon_R' = 1 + \frac{a_2}{k_2} \cdot log\left(\frac{V_2}{V_1}\right) = 1 + k \cdot log\left(\frac{V_M}{V_{REF}}\right) \tag{2.14}$$

The expression on the right side of equation 2.14 is the published formula by Denoth [5].

The absolute values of the elements in the circuit such as the coil and the capacitors, are not influencing the measurement.

The drawback with this approach is that the diode capacitance $C_D = f(V)$ is assumed to be linear for the logarithm of the voltage (figure 2.7) for a certain range. The task is to investigate this allegation. However, an alternative formula concerning the change of the capacitance in the resonant circuit and its relation to the relative permittivity ε_R' is derived with the following equations.

The general formula for the capacitance C_D of a varactor diode is given by

$$C_D = \frac{C_0}{\left(1 + \frac{V}{V_D}\right)^{\gamma}} \tag{2.15}$$

with V as the DC voltage applied to the diode and V_D as the diffusion voltage. C_0 is the capacitance of the diode at $V = 0V$. The exponent in the denominator is expected to be 0,5 for a diode with uniformly and constant doped p- and n-regions. For any other kind of doped varicap, the exponent may have values between 0,3 and 2,0.

For the total capacitance in the resonant circuit it is correct to say

$$C = C_S + \frac{C_0}{\left(1 + \frac{V_1}{V_D}\right)^{\gamma}} = (\varepsilon_R' - j\varepsilon_R'')\mathrm{C_S} + \frac{C_0}{\left(1 + \frac{V_2}{V_D}\right)^{\gamma}} \tag{2.16}$$

and

$$\Delta C = C_1 - C_2 = \frac{C_0}{\left(1 + \frac{V_1}{V_D}\right)^{\gamma}} - \frac{C_0}{\left(1 + \frac{V_2}{V_D}\right)^{\gamma}} = (\varepsilon_R' - j\varepsilon_R'')\mathrm{C_S} - C_S \tag{2.17}$$

or

$$\Delta C = C_1 - C_2 = \frac{C_0}{\left(1 + \frac{V_1}{V_D}\right)^{\gamma}} - \frac{C_0}{\left(1 + \frac{V_2}{V_D}\right)^{\gamma}} = (\varepsilon_R' - 1)\mathrm{C_S} - j\varepsilon_R'' C_S \tag{2.18}$$

If one considers the real part only, this yields

$$\Delta C = (\varepsilon_R' - 1)\mathrm{C_S} \tag{2.19}$$

and

$$\varepsilon_R' = \frac{\Delta C}{C_S} + 1 \tag{2.20}$$

Note: Rearranging the equation gives the exponent

$$\gamma = \frac{\log\left(\frac{C_1}{C_2}\right)}{\log\left(1 + \frac{V_2}{V_D}\right) - \log\left(1 + \frac{V_1}{V_D}\right)} \tag{2.21}$$

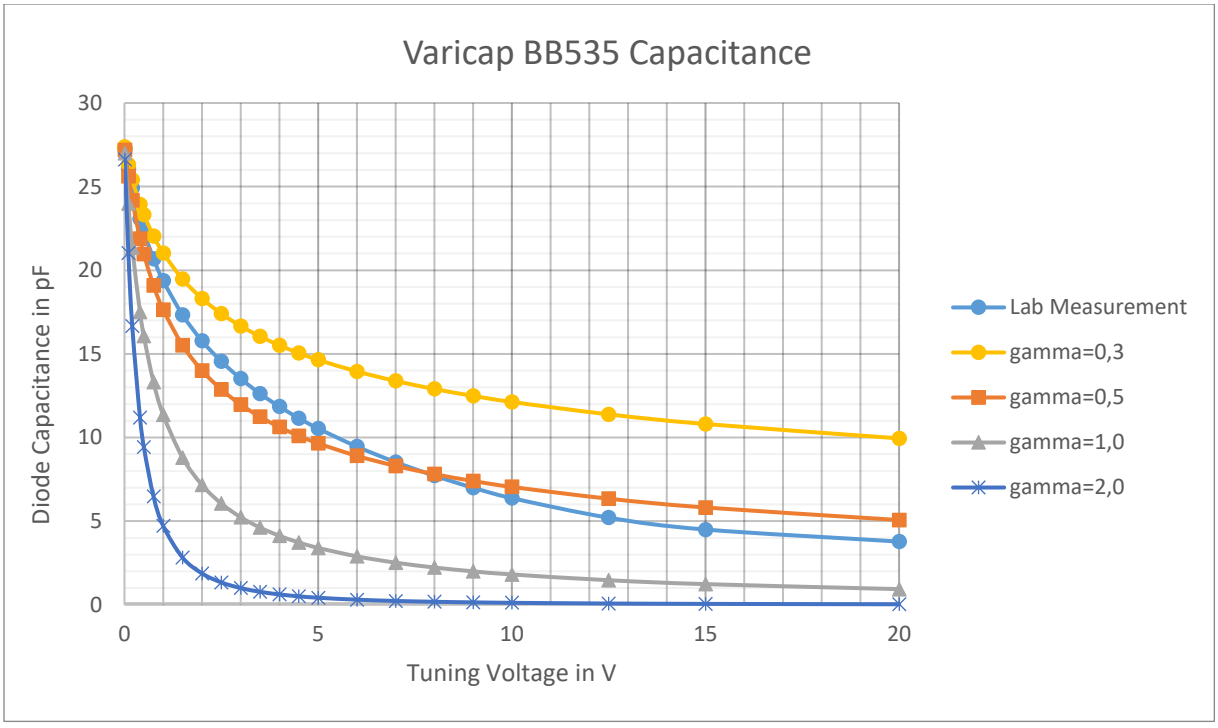

Figure 2.8: Comparison of different ways to obtain C_{Diode}

The diagram shows the difference between the real diode capacitance which was measured in the lab and the diode capacitance that is calculated with the general formula (equation 2.15). One can observe that the BB535 varicap does not comply with the calculated curves. A diagram with logarithmic scaled x-axis is in appendix A. The functionality of the currently used diode is proved in the final experiment in section 4.3.

2.5. Calibration

The sensor can be calibrated with solid state or liquid standard dielectric materials, with a known relative permittivity. Some materials are exemplarily listed in table 2.1:

Table 2.1: List of dielectric materials

Dielectric material	Dielectric constant ε'_R
Air (dry)	1,0006
Plywood *	2,75
Varnished wood *	4,01
Unknown plastic *	2,26
Sponge, dry *	1,02
Sponge, wet *	4,25
Polyvinylchloride PVC	3,4
Polyethylene PE	2,3
Polypropylene PP	1,5
Paraffin	2,2
Panasonic FR4 (1MHz)	5,4
Farnell C.I.F. FR4 (1MHz)	4,7
Ice (f >100kHz, T = -20°C)	3,2

Those materials which are marked with an asterisk are measured in the laboratory with the prototype sensor and an impedance analyzer. Those dielectric constants are determined by a reference measurement of the sensor capacitance exposed to air ($C_{SENSOR} = 700fF$) compared to the sensor exposed to the material in the list. The back plane is attached to the guard input of the analyzer to eliminate the influence of the capacitance of each electrode to the plane. The impedance is measured differentially at the electrodes. The corresponding parallel capacitances are calculated by the analyzer.

Other materials and compounds of this list could be utilized on some future occasion. They are a choice in terms of availability, purity and homogeneity. The permittivity can be determined with datasheets as it is exemplarily done in the table above. Those calibration materials will be more accurate than the ones used for the current project. Some measurements of reference materials with the LCR impedance analyzer are shown on the appendix A.3. The measurement was carried out in the same series of tests as the capacitance measurement of the sensor in the previous section 2.1, thus the test configuration remains the same that the results are comparable. The reference value with air as dielectric material is $C_{Sens} = 705fF$. The tests were carried out at a frequency of 300kHz and a voltage of 500mV to avoid measurement errors.

2.6. Notch Transfer Function

The first approach to analyze the sensor circuit is to investigate the transfer function. The circuit is redrawn and evaluated by calculating currents and voltages, nodes and meshes. The coupling capacitors with $C_3 = C_7 = 10\text{nF}$ are neglected for simplicity. Their reactance at 20Mhz is very small which will not influence the conclusion about the transfer function.

$$X_{C3} = \frac{1}{2\pi f C} = 0{,}79\Omega \tag{2.22}$$

The capacitances and the inductance of the branches are substituted by their equivalent impedances Z_1 and Z_2 to set up the equations in a convenient form. It is important to mention that at this stage of the circuit analysis, other parasitics, i.e. the series resistance of the inductor, are not considered yet.

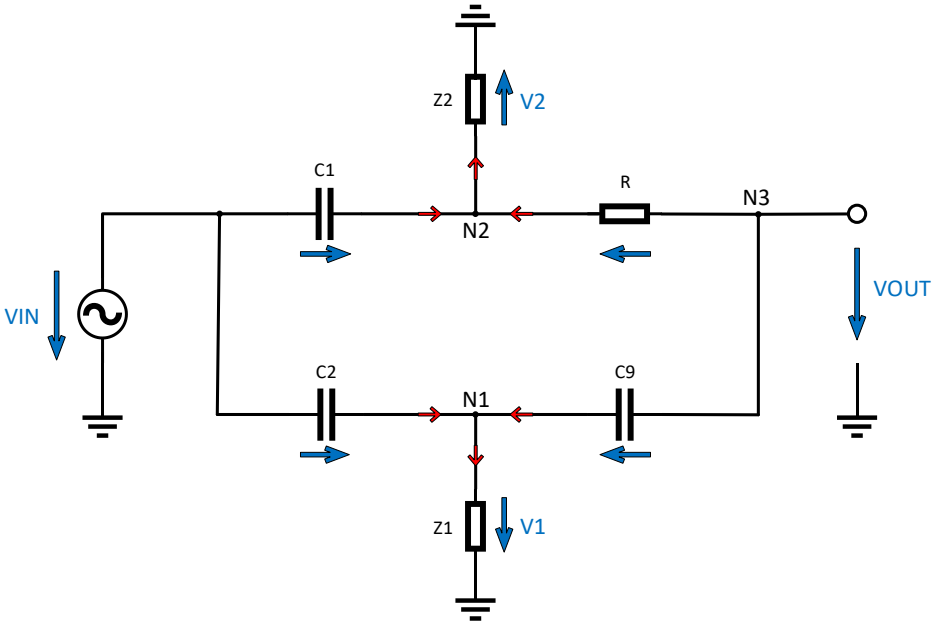

Figure 2.9: Equivalent circuit of the notch filter

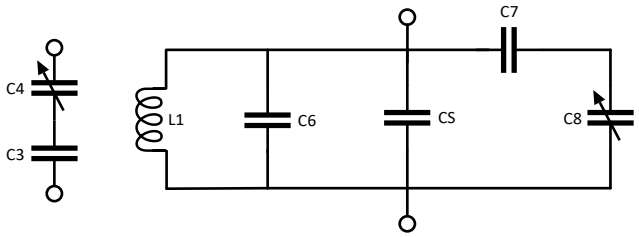

Figure 2.10: Equivalent circuits of the upper and the lower T-branch, Z_2 and Z_1, respectively

Note: The original circuit has an extra capacitance $C_6 = 20pF$ in parallel to the sensor capacitance. It is the parasitic capacitance of the floating back plane that increases the total capacitance of the resonant circuit. The sensor is predefined with $C_S = 1pF$, the diodes with each $C_D = 18{,}7pF$. The other values remain as they are originally dimensioned.

Node equations according to figure 2.9 are:

$$N_1: \quad (V_{in} - V_1) \cdot sC_2 + (V_{out} - V_1) \cdot sC_9 - \frac{V_1}{Z_1} = 0 \tag{2.23}$$

$$N_2: \quad (V_{in} - V_2) \cdot sC_1 + \frac{V_{out} - V_2}{R} - \frac{V_2}{Z_2} = 0 \tag{2.24}$$

$$N_3: \quad \frac{V_2 - V_{out}}{R} + (V_1 - V_{out}) \cdot sC_9 = 0 \tag{2.25}$$

The voltages V_1 and V_2 that drop at the impedances of the T-branches Z_1 and Z_2 can be isolated in equations N_1 and N_2. The results substitute V_1 and V_2 in equation N_3:

$$N_3: \quad \frac{V_{in}sC_1 + \frac{V_{out}}{R}}{sRC_1 + 1 + \frac{R}{Z_2}} - \frac{V_{out}}{R} + \frac{V_{in}s^2C_2C_9 + V_{out}s^2C_9^2}{s(C_9 + C_2) + \frac{1}{Z_1}} - V_{out}sC_9 = 0 \tag{2.26}$$

The equation must be rearranged to separate V_{IN} and V_{OUT} to get the typical form of a transfer function H(s)

$$V_{in}\left[\frac{sC_1}{sRC_1 + 1 + \frac{R}{Z_2}} + \frac{s^2C_2C_9}{s(C_9 + C_2) + \frac{1}{Z_1}}\right] = V_{out}\left[-\frac{\frac{1}{R}}{sRC_1 + 1 + \frac{R}{Z_2}} + \frac{1}{R} - \frac{s^2C_9^2}{s(C_9 + C_2) + \frac{1}{Z_1}} + sC_9\right] \tag{2.27}$$

Modification of this equation yields

$$H(s) = \frac{V_{out}}{V_{in}} = \frac{\frac{sC_1}{sRC_1 + 1 + \frac{R}{Z_2}} + \frac{s^2 C_2 C_9}{s(C_9 + C_2) + \frac{1}{Z_1}}}{-\frac{\frac{1}{R}}{sRC_1 + 1 + \frac{R}{Z_2}} + \frac{1}{R} - \frac{s^2 C_9^2}{s(C_9 + C_2) + \frac{1}{Z_1}} + sC_9} \tag{2.28}$$

The transfer function has become very complicated. There conclusions about the circuits behavior can be drawn at this stage of the calculation.

The terms for Z_1 and Z_2 are set up separately according to figure 2.10:

$$Z_2 = \frac{1}{sC_4} \tag{2.29}$$

$$Z_1 = \frac{sL_1}{1 + s^2 L_1 (C_6 + C_8 + C_{Sensor})} \tag{2.30}$$

Substitution and simplification yields:

$$H(s) = \frac{\frac{sC}{1 + sR(C + C_4)} + \frac{s^3 LC^2}{1 + s^2 L(2C + C_6 + C_8 + C_{Sensor})}}{\frac{1}{R} + sC - \frac{1}{R + sR^2(C + C_4)} - \frac{s^2 C^2}{1 + s^2 L(2C + C_6 + C_8 + C_{Sensor})}} \tag{2.31}$$

This equation is further simplified and rearranged in such a way that a general form of a known transfer function (equation 2.32) could be compared.

However, no assumptions can be made on this transfer function.

Equation 2.31 is entered in a MATLAB script, solved with the original component values and plotted as a bode diagram

.

Frequency response of the notch circuit:

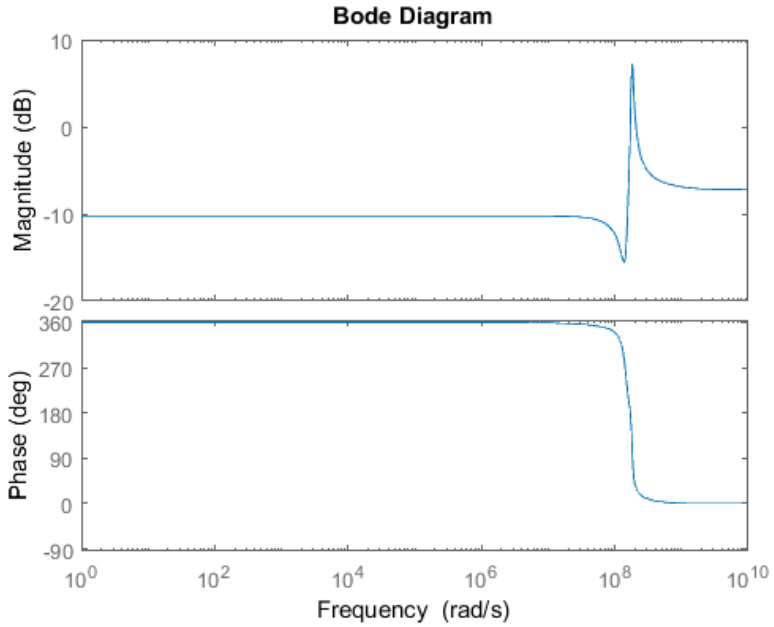

Figure 2.11: Bode diagram of the notch filter without consideration of parasitics and C_6

One can observe that the output is attenuated by more than 10dB and that there is a sharp minimum followed by a sharp peak beyond 10^8 radians per second (f>16MHz).

A zoom into diagram shows that the sensor circuit behaves as a highpass notch filter:

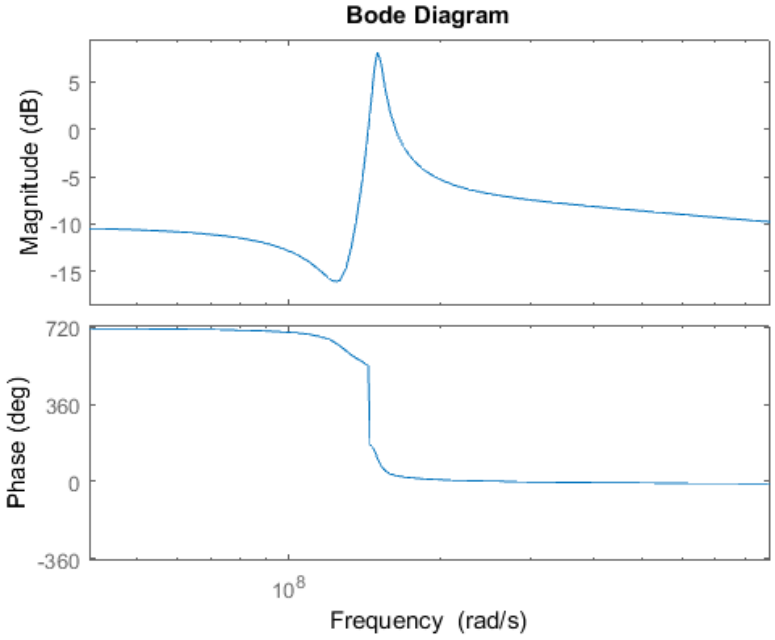

Figure 2.12: Zoom into the Bode plot of the high pass notch (no parasitics considered, except C_6)

The calculation result for figure 2.12 is obtained without respect to the parasitic capacitance of the floating backplane C_6, in contrast to figure 2.11: One can observe that the resonance

frequency has slightly decreased while the shape of the peak remains unchanged. The peak which follows the minimum is not expected to be of such a high magnitude. Therefore, and to get more accurate results, parasitics, especially the resistance in the resonant circuit, must be considered.

A highpass notch filter has a general transfer function analogical to a bandpass filter transfer function, except a different numerator:

$$H(s) = \frac{H_0 \cdot (s^2 + \omega_z^2)}{s^2 + s\frac{\omega_0}{Q} + \omega_0^2} \tag{2.32}$$

where ω_0 names the angular frequency where the filter peaks.

H_0 defined as the gain of the circuit depending on the quality factor of the filter that is given by the bandwidth:

$$H_0 = \frac{H}{Q} \tag{2.33}$$

$$Q = \frac{f_0}{B} \tag{2.34}$$

As usual, the bandwidth is determined by the corner frequencies at -3dB. Notch filters have a very narrow band response. Q must be high that the corner frequencies are very close to each other.

A notch has one out of three possible characteristics: highpass, lowpass or standard [6]. It is determined by the relation of the pole frequency ω_0 and the zero frequency ω_z.

For the standard ω_0 equals ω_z, for the lowpass the zero frequency is greater and for the highpass filter the pole frequency is greater. Unfortunately, this could not be observed in at a first glance (equation 2.31) but it's obviously identifiable if one compares figure 2.12, figure 2.16 and figure A.4.

2.7. Spice Simulation

To get more revealing information, the sensor circuit needs to be investigated by simulations. The favorable tool for this purpose is OrCAD Capture. Besides, the simulation verifies the transfer function calculation result from the previous chapter.

Simulation schematic:

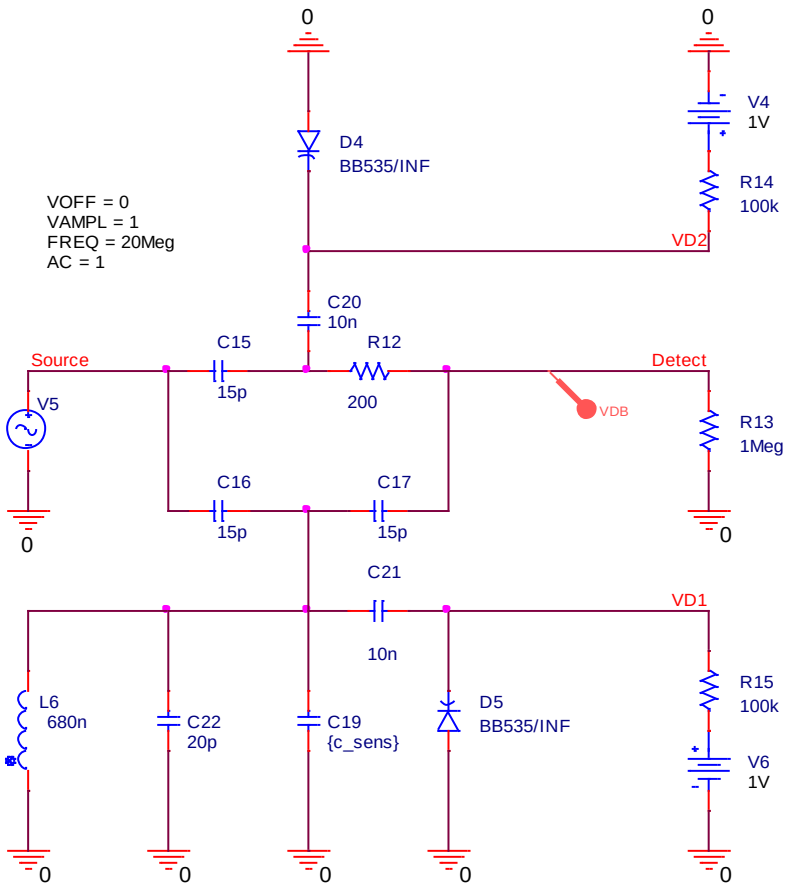

Figure 2.13: Schematic of the sensor circuit (no parasitics considered)

Figure 2.13 depicts the circuit that is revised and updated compared to the previous section. The capacitors, here denoted with C_{20} and C_{21}, are necessary to decouple the DC voltage from the small signal. The blocking resistors R_{14} and R_{15} prevent AC signals to be shorted by the 0Ω-resistance of the voltage sources V_4 and V_6. The latter are adjusted with 1V each (default configuration). This corresponds to the diode's minimum of its operating range according to the datasheet. The diode model is directly imported from the manufacturer. The sensor capacitance is defined with $C_{SENS} = 1pF$. It is a tradeoff between the previous measurements with the impedance analyzer and the simulated results by the Sonnet software. The dielectric constant is determined to be $\varepsilon_R = 1$ to simulate the sensor exposed to air to get reference values. An AC simulation is performed to determine the frequency response of the circuit.

Bode plot according to the schematic in figure 2.13, zoomed in:

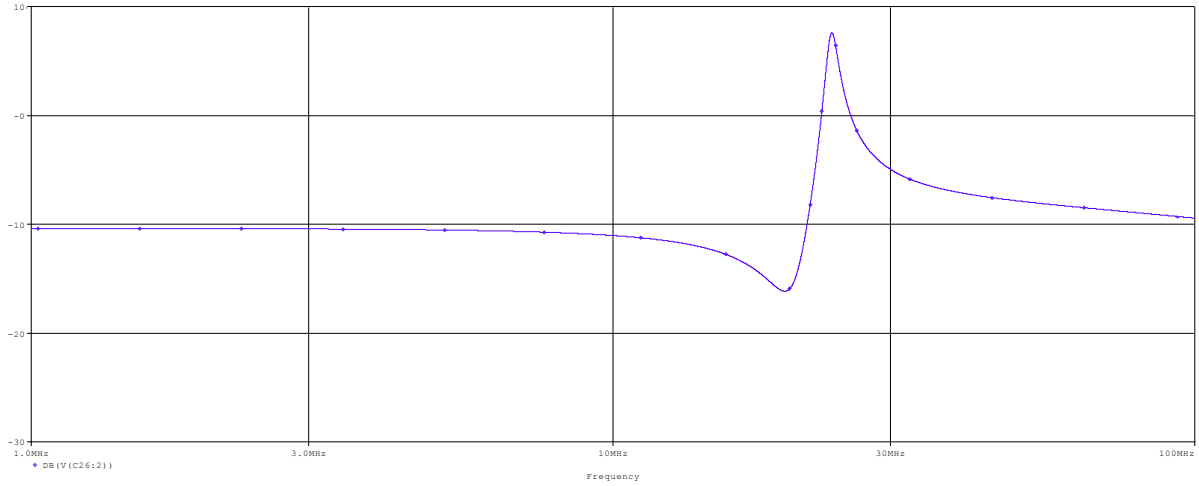

Figure 2.14: Notch frequency response without parasitics

Measuring the minimum with the cursor functions gives a frequency of $f_{res} = 19{,}738MHz$.

The calculation results of section 2.6 (figure 2.12) are confirmed, hereafter parasitics will be considered.

First, the resistance of the source path and the line inductance are inserted. Their values are chosen by experience with $R = 50\Omega$ and $L = 100nH$.

The SRR1050A series is a shielded power inductor from the manufacturer Bourns. It has a nominal inductance of 680nH, a tolerance of 30% and a self-resonant frequency of 110MHz. The component has been chosen due to its good properties. The series resistance at DC conditions is in the Milliohm-range which gives a very good quality factor. The distributor of the inductor promises a quality factor of $Q = 221$. This exceeds other available inductors by far.

The quality factor Q must be high to achieve the narrowest resonance peak possible. For a parallel resonant circuit, Q and the bandwidth B are defined as

$$Q = 2\pi f_0 CR = R\sqrt{\frac{C}{L}} \tag{2.35}$$

$$B = f_{C1} - f_{C2} = \frac{f_0}{Q} \tag{2.36}$$

with f_0 as the resonant frequency.

Bourns offers an equivalent circuit of the realistic inductor for simulation purposes. It is inserted in the following schematic, and it considers the parallel resistance and the parallel capacitance of the coil. The series resistance is given at DC conditions.

The inductor is evaluated with the impedance analyzer:

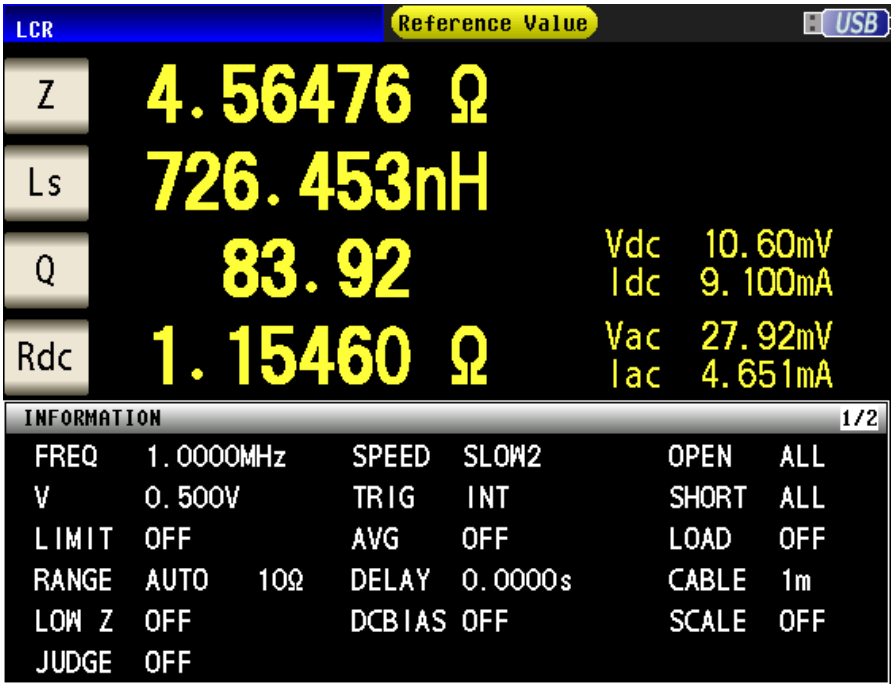

Figure 2.15: Key figures of Bourns SRR1050A shielded power inductor

It is very interesting to observe that the inductor's DC resistance $R_{DC} = 1{,}15\Omega$ is 255 times higher than denoted in the datasheet. The inductance with L = 726nH is within the tolerance. These metered values are preferred instead of the nominal values of the datasheet. They will be considered for further calculations and simulations to have comparable results to the real circuit configuration in the lab.

Currently the coil is used in the high frequency range, hence the skin effect must be considered. A MATLAB script helps to determine the real series resistance of the coil. For quasi stationary fields in cylindrical conductors it is possible to derive Bessel's differential equations with Bessel functions as general solutions. The penetration depth δ of the current and subsequently the ratio $\frac{R_S}{R_{DC}}$ can be calculated [7].

$$\delta = \sqrt{\frac{2}{2\pi \cdot f \cdot \mu_0 \cdot \gamma}} = 15\mu m \tag{2.37}$$

with the conductance of copper $\gamma = 56\frac{MS}{m}$ and the vacuum permeability $\mu_0 = 4\pi \cdot 10^{-7}\frac{H}{m}$. The radius of the copper wire is measured with $r_0 = 0{,}2\text{mm}$.

The ratio of the radius and the penetration depth equals the ratio of the real resistance and the nominal resistance:

$$\frac{R}{R_0} = \frac{r_0}{2\delta} = \frac{0{,}2 \cdot 10^{-3}}{2 \cdot 1{,}5039 \cdot 10^{-5}} = 6{,}7 \tag{2.38}$$

This yields the real series resistance of the inductor at 20MHz:

$$R_S = 6{,}7 \cdot R_{DC} = 7{,}7\Omega. \tag{2.39}$$

The coil has another property that increases parasitic effects: the ferrite core. It can be considered by calculating the effective permeability. It is depending on the geometry and material of the core. Unfortunately, the datasheet does not provide these information, thus the calculation is skipped. The influence of the core on the series resistance is estimated by simulating the circuit and comparing the bode plot with measured frequency response. The latter will be obtained with a test setup in the laboratory (section 2.8).

The manufacturer provides the parallel capacitance with $C_P = 544fF$ and the parallel resistance with $C_P = 1003\Omega$. The updated schematic includes the equivalent circuit of the inductor with new parameters (figure 2.16).

Figure 2.16 shows the difference of the impact of the ideal (red) and the realistic (green) inductor model on the frequency response: The minimum turns out to be a sharp peak and the maximum is obviously flattened. The resonance frequency is measured with a cursor at $f_{RES} = 20{,}096\text{MHz}$ where amplitude $\text{V}_{\text{OUT}} = 25{,}4\text{mV}$.

The signal in the passband is attenuated by $-10{,}4dB$. If a 3V signal at the input, there is only a 300mV voltage drop in the passband and at the minimum, voltage values will be range of a few millivolts. This will be considered in more detail (section 4).

The magnitude response in the following picture shows the difference of the circuit with the ideal inductor (figure 2.13) with nominal values and the adapted circuit with the extended coil model parameters (figure 2.17):

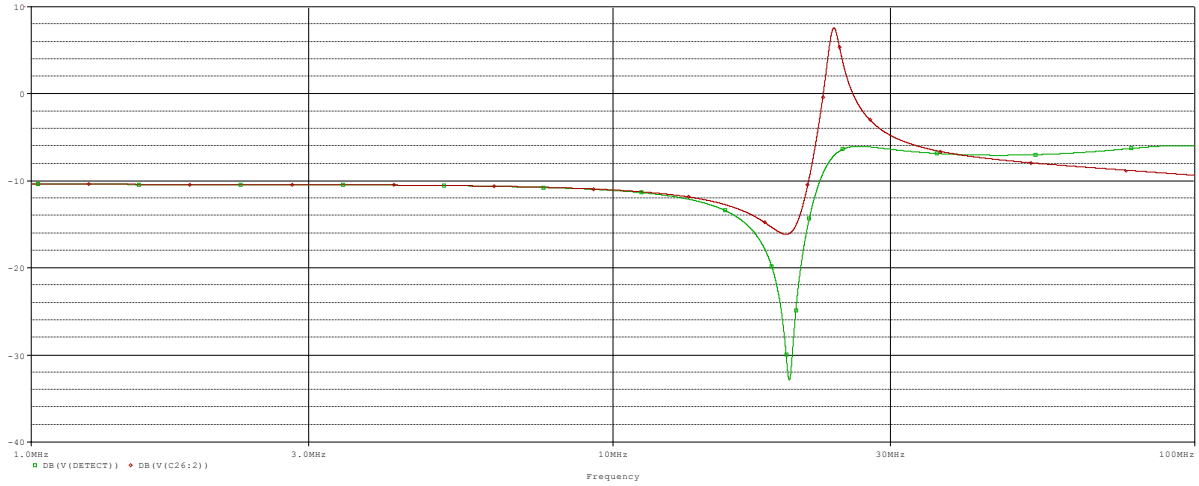

Figure 2.16: Simulation of the sensor with and without parasitic effects of the inductor

Updated simulation schematic:

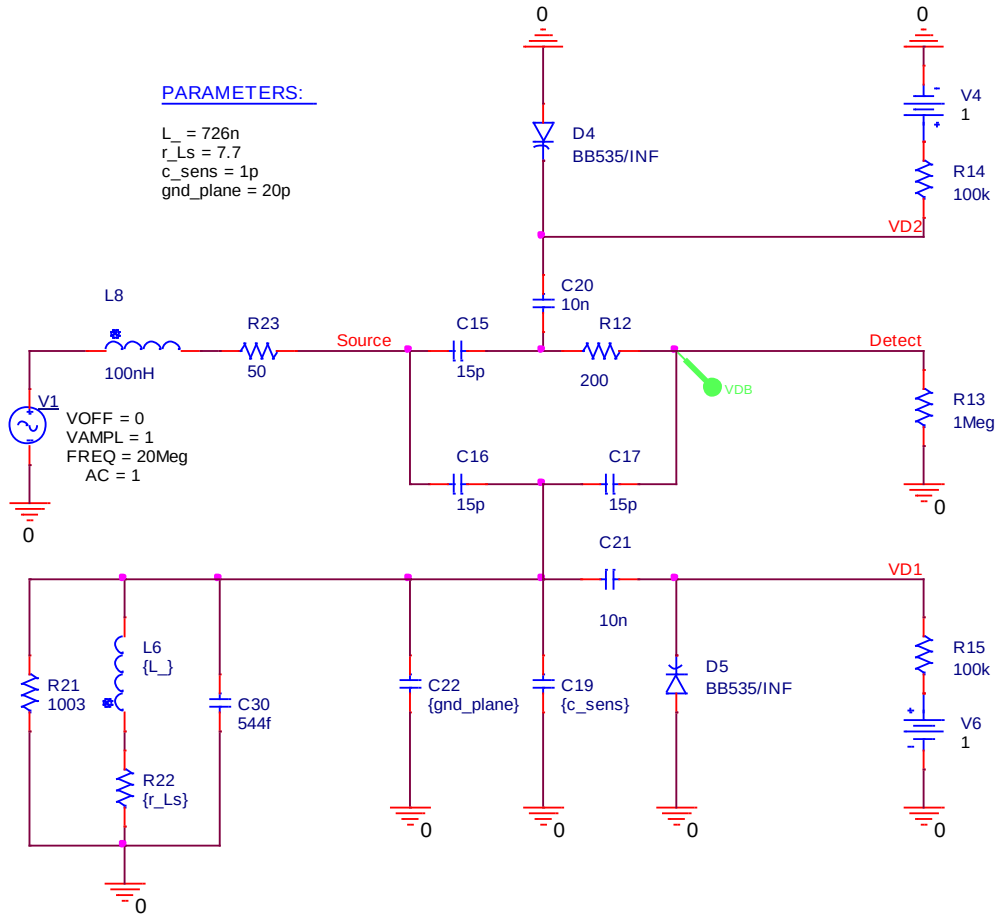

Figure 2.17: Simulation with new parameters of the inductor and the line impedance of the AC source

2.8. Notch Prototype

A prototype of the notch is designed with Altium Designer 16.1. and fabricated with the copy milling machine on 1.6mm double sided PCB with an FR4 dielectric. The bill of materials is listed in table B.1.

Altium 3D-model:

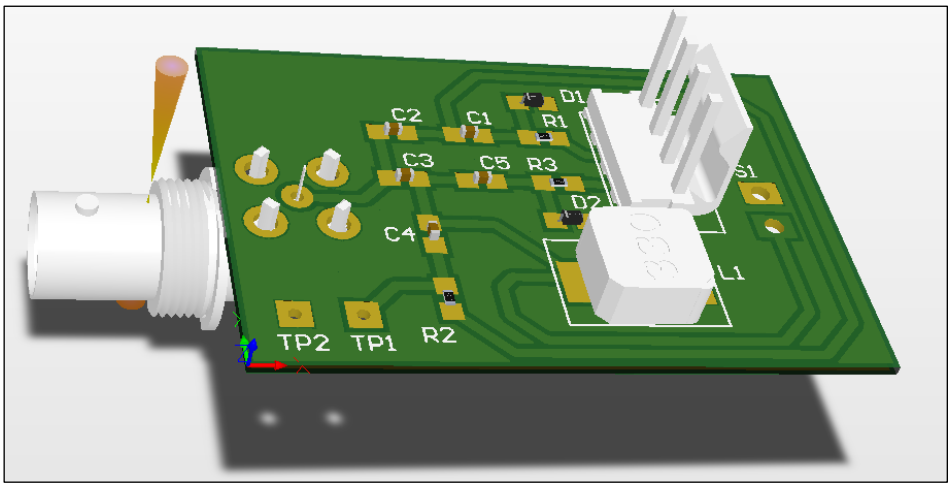

Figure 2.18: Notch circuit prototype

Initially, the circuit will be sourced by a signal generator with a 20Mhz sine wave signal. A BNC connector is mounted on the board to use a 50Ω coaxial cable to maintain the integrity of the AC signal. The DC signals for the tuning diodes are adjusted with a DC power supply unit. The tuning voltages are connected to the header pins. The sensor connects directly to S_1 with a two-pin header to avoid as much parasitic effects, i.e. wire inductance, as possible.

The prototype is connected to the AC and DC signal source and measured with digital oscilloscope (200MHz, 5GSa/s) according to the following parameters.

- AC, sinewave: $V_{in} = 1V_{pp}$, $f = 20MHz$
- DC: $V_{D1} = 1V$, $V_{D2} = 1V$
- Measurement: FFT, max hold
- Resolution bandwidth: $RBW = 75kHz$
- Bin size = $19.1kHz$,
- Window: Hanning
- Sweep time: $600s$

One can observe that the frequency response of the laboratory test setup is very similar to the frequency response of the simulated circuit (table 2.2)

FFT with oscilloscope, max hold:

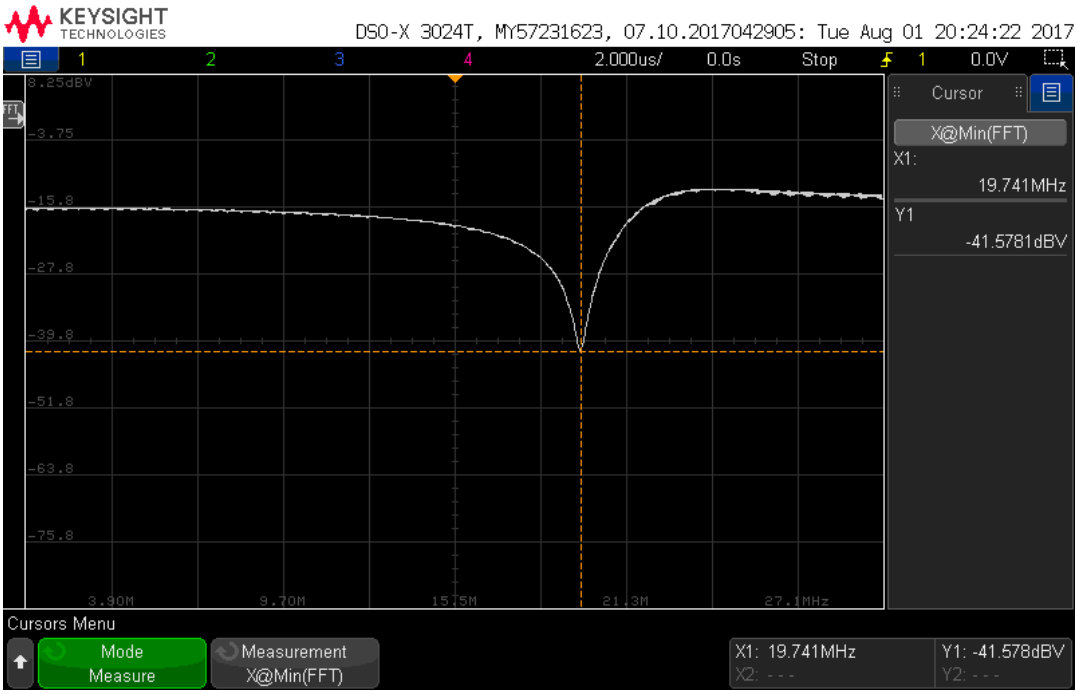

Figure 2.19: Frequency response of the prototype notch circuit (linear scaled x-axis)

AC simulation, frequency sweep:

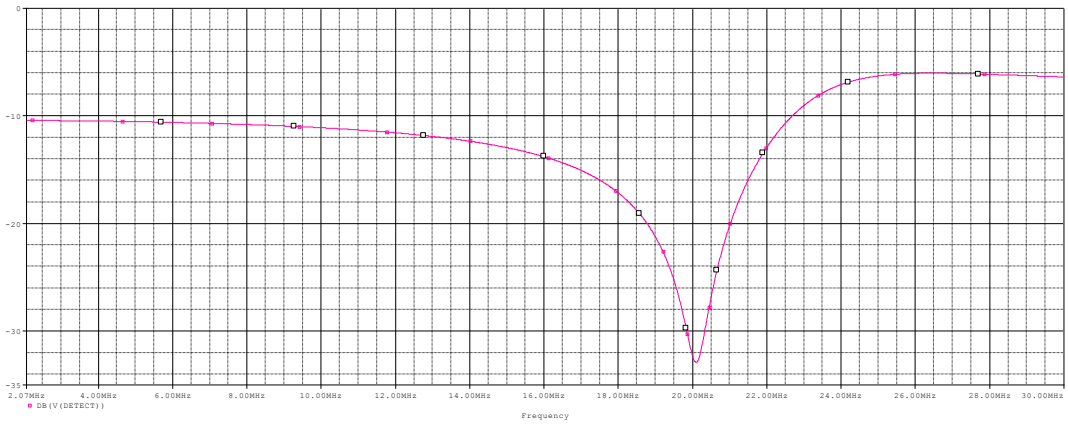

Figure 2.20: Notch filter, magnitude response (linear scaled x-axis)

The simulation result is based on the schematic in figure 2.17.

Table 2.2: Frequency response measurement

Measurement type	f_{res} in MHz	V_{out} in dBV	**Attenuation** in dB
Simulation (fig.2.20)	20,099	-41,57	-10,5
Laboratory (fig.2.19)	19,741	-32,91	-15,8

3. Key Figures

The key figures of the sensor circuit need to be investigated to understand its functionality and limits. The following tasks are performed with Spice simulations compared to prototype tests and measurements in the laboratory.

Experimental measurements are performed with:

- 7,5GHz spectral analyzer
  - with a high frequency probe
  - in a 50Ω-network
- 100Mhz digital oscilloscope with a 10MΩ passive probe
- 6GHz digital oscilloscope with a 10MΩ passive probe

The HF probe is actively powered by the spectral analyzer, yet it is attenuating the measured signal by -13,45dB. The probe measurement is plotted in the appendix A.5.

3.1. Calibration with Air

The default settings of the tuning voltages for the following measurement series are evaluated with the first test. Therefore, the sensor is mounted on a bracket and exposed to air as a reference medium.

The input sensor circuit is connected to the spectral analyzer with a coaxial cable and a frequency sweep is performed. The back plane is floating. The minimum output voltage at $f_{OUT} = 20MHz$ must be searched by adjusting the tuning voltages, the loss compensation is pre-set to $V_{D2} = 1V$ and the stress resultant V_{D1} is noted as the reference voltage V_{REF}. The measurement results of the calibration process are listed in the table below. Those values are the reference values for the following tests.

Table 3.1: Calibration and reference data

V_{D1} (V_{ref}) in V	V_{D2} in V	f_{out} in MHz	P_{out} in dBm	V_{out} in mV
1,136	1,0	20,0	-36,63	4,66

The DC tuning voltages are monitored with a handheld multimeter. The output power is measured with the spectral analyzer and corrected by the attenuation of the probe. The amplitude of the output voltage is calculated.

The capacitance in the resonance circuit increases dramatically if the backplane is connected. The output frequency drifts to $f_{out} = 18{,}84MHz$. The spectral analyzer also shows a second resonance minimum at $f_{out} = 29{,}24MHz$ because of the inductance of the wiring (figure A.6). Both effects are unwanted, thus the backplane remains disconnected.

3.2. Output Characteristics

The output frequency changes when different values for the relative permittivity are applied. The amplitude changes, if losses occur. The question is, how much does the output change and is the dependency between input and output linear?

3.2.1. Frequency

The circuit is simulated with different values for the sensor capacitance. The parameter is swept from 1pF ($\varepsilon_R' = 1$, reference value) to 5pF ($\varepsilon_R' = 5$, estimated maximum). Some of the calibration materials which are listed in table 2.1, (section 2.5) are simulated as well.

AC simulation, parameter sweep of C_{SENSOR}:

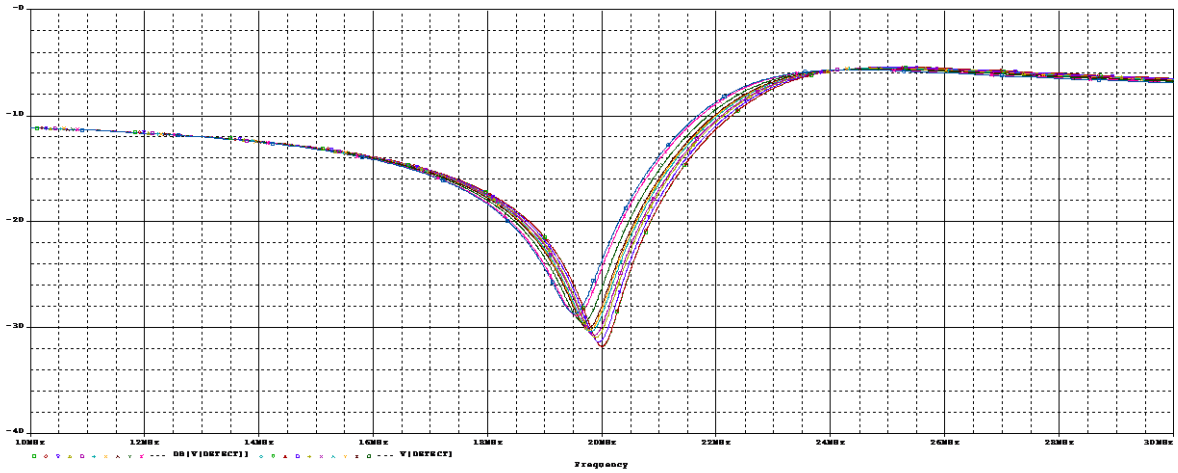

Figure 3.2: Output frequency at different sensor capacitances

The output frequency gets lower and the output voltage gets higher as the dielectric constant increases. Those deviations for different ε_R are listed in the table below.

Table 3.2: Output curve cursor measurements

ε_R'	f_{out}	Δf	V_{out}	V_{out}	Material
	in MHz	in kHz	in dBV	in mV	
1	19,999	0	-30,806	28,82	air
1,02	19,997	2	-31,788	25,74	dry sponge
1,5	19,943	56	-31,379	26,98	Polypropylene, dry snow
2	19,877	122	-30,974	28,27	
2,26	19,857	142	-30,771	28,94	unknown type of plastic
3	19,775	224	-30,221	30,83	wet snow
3,2	19,753	246	-30,079	31,34	ice
4	19,665	334	-29,535	33,36	varnished wood
5	19,557	442	-28,904	35,88	

Note: V_{D1}=1,035V (calibrated), V_{D2}=1V (default).

Output characteristic of the Denoth sensor:

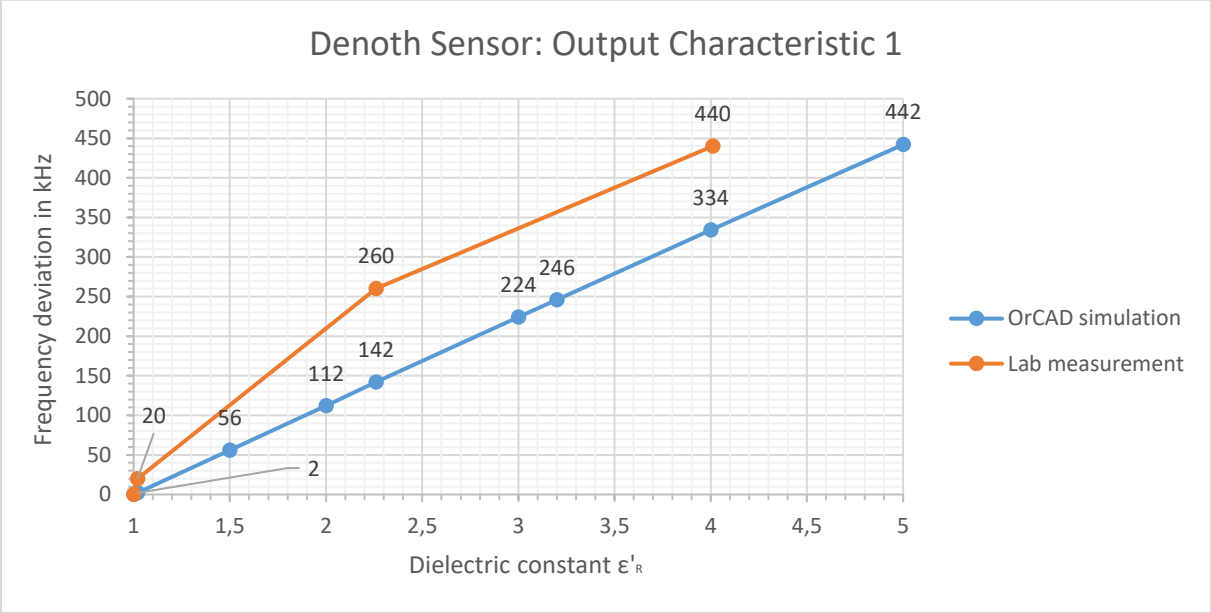

Figure 3.3: Simulation vs. laboratory measurement

The simulation promises a linear output response to a change of the relative permittivity of the sensor dielectric. Unfortunately, these results could not be confirmed with the lab experiment, most probably because of the inaccurate permittivity measurements of the calibration materials and deviations of the measurement configurations. The acquisition of different matter with known dielectric parameters (reliable datasheets) and suitable shape and size (14cm*13cm*3cm) will be essential for the development of a good quality product. The measurement table is in appendix B.3.

A follow-up question is how to calculate of the resonance frequency or the relative permittivity, respectively. If the general formula for parallel resonance circuits is applicable to the current layout, these equations must comply:

$$f_0 = \frac{1}{2\pi\sqrt{LC}} = 20MHz \tag{3.1}$$

According to table 3.2, one expects to calculate a relative permittivity $\varepsilon'_R = 5$ for a frequency drift $\Delta f = 442kHz$:

$$f_1 = f_0 - \Delta f = \frac{1}{2\pi\sqrt{LC + \Delta C}} = 19{,}557MHz \tag{3.2}$$

To calculate ε' follows:

$$\frac{f_0}{f_1} = \frac{\frac{1}{2\pi\sqrt{LC}}}{\frac{1}{2\pi\sqrt{LC+\Delta C}}} = \frac{\sqrt{C+\Delta C}}{\sqrt{C}} \qquad \Rightarrow \qquad \left(\frac{f_0}{f_1}\right)^2 = \varepsilon_R' \tag{3.2}$$

The equation yields $\varepsilon_R' = 1{,}045$ instead of $\varepsilon_R' = 5$.

The proof that the general formula is not applicable is given, if the simulation results for f_0 and f_1 are inserted.

3.2.2. Amplitude

The simulation schematic is extended with an ohmic resistor parallel to the sensor capacitance to simulate the polarization losses ε''. The impact on the sensor output is documented in this section.

The impedance of the sensor and the loss resistor is given by:

$$Z_C = \frac{1}{sC_S + \frac{1}{R_L}} \tag{3.3}$$

The admittance of the sensor capacitance equals the permittivity multiplied with the sensor constant k:

$$Y_C = sC_S + \frac{1}{R_L} = \varepsilon_0 k_1 \cdot (\varepsilon_R' - j\varepsilon_R'')j\omega \tag{3.4}$$

$$Y_C = j\omega C_S + \frac{1}{R_L} = j\omega k_1 \varepsilon_R' + \mathrm{k_1}\omega\varepsilon_\mathrm{R}''\varepsilon_0 \tag{3.5}$$

Separation of the real from the imaginary part yields

$$R_L = \frac{1}{\mathrm{k_1}\omega\varepsilon_\mathrm{R}''\varepsilon_0} \tag{3.6}$$

Constant k_1 is derived as

$$k_1 = \frac{C_S + C_B}{\varepsilon_0} = \frac{22 \cdot 10^{-12}}{8{,}854 \cdot 10^{-12}} = 2.4848 \tag{3.7}$$

If one considers reasonable losses for different samples of wet snow between $\varepsilon'' = 0{,}01$ and $\varepsilon'' = 0{,}4$ [9] and equation 3.6, the loss resistor must be in the range of $36k\Omega > R_L > 900\Omega$.

AC simulation, sweep R_L (loss resistor value):

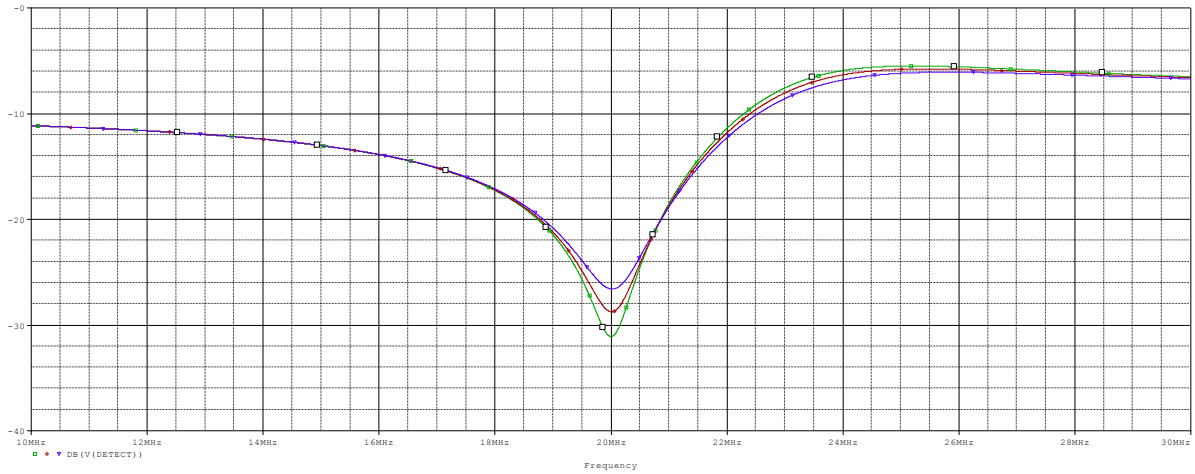

Figure 3.4: Simulation of polarization losses on the output voltage

Losses change the amplitude of the output voltage, the effect on output frequency is negligibly small. If the losses are high (resistor value low, thus current high), the output amplitude is higher. With the varactor diode in the upper T-branch, this deviation must be compensated to keep the output voltage at the calibrated minimum. The cursor measurements of this simulation are listed in table 3.3.

It is obvious that the loss compensation is a very sensitive process. This needs to be considered for the choice of the ADC. (discussed in detail in section 4.3).

Graphical representation of table 3.3:

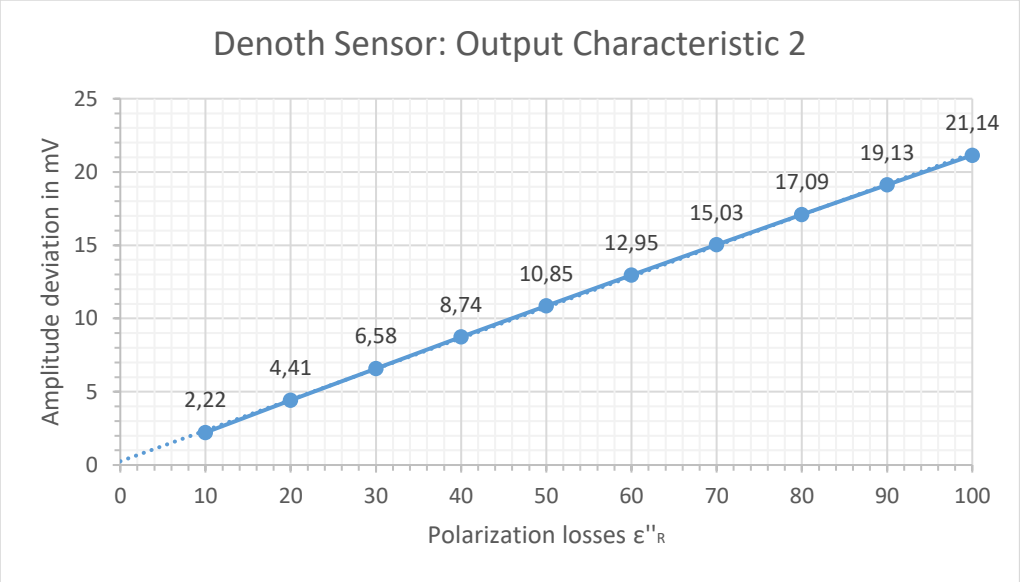

Figure 3.5: Linear relation of losses and output voltage

The analysis of the recent simulation shows the linear dependency between the output amplitude and losses. The measurements are documented in appendix B5.

The original paper [5] does not provide a method or formula to compute the imaginary part. It is assumed to be determined empirically. It is possible to generate a calibration curve with well-known lossy materials that can be implemented as a look-up table for the microcontroller. Another possibility is to calculate ε_R'' with the quality factor of the resonant circuit [3]. This method is not evaluated with this thesis, nevertheless it is an interesting approach for future projects.

3.3. Tuning Range

The frequency and amplitude of the output voltage changes when the tuning voltages are altered. The capacitance in the T-branches decreases with increasing V_{D1} or V_{D2}. The corners at 5V are evaluated to determine the tuning capability of those varactor diodes.

AC simulation, sweep voltage source V_{D1} at varicap 1:

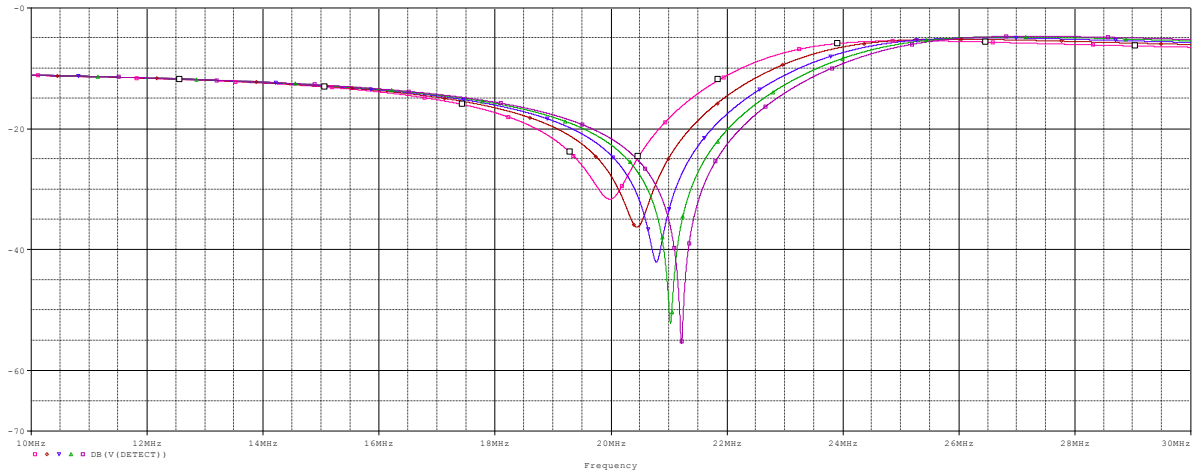

Figure 3.6: Output frequency deviation because of V_{D1}

AC simulation, sweep voltage source V_{D2} at varicap 2:

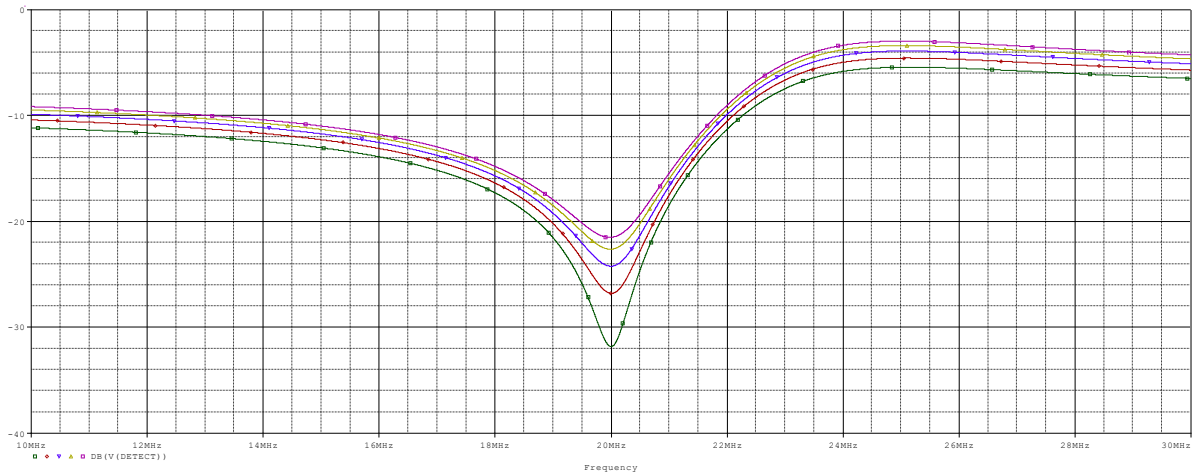

Figure 3.7: Output amplitude deviation because of V_{D2}

The diagrams show how much the frequency and the amplitude of the output voltage can be influenced by decreasing the capacitance of the varactor diodes. The maximum DC voltage is determined with 5V. The maximum compensation of frequency is $\Delta f = 1{,}236 MHz$. The maximum compensation of amplitude is $\Delta V = 58{,}5 mV$.

An experiment to visualize the tuning capability of the varactor diodes is carried out in the laboratory. The prototype circuit is connected to the spectral analyzer and a frequency sweep is performed. Tuning voltage U_1 is incremented from 0 to 5V in steps of 0,5V. The output

voltage is adjusted by tuning U_2 at the minimum (~80dBm). The corresponding output frequency is noted in table 3.4 and plotted against U_1.

Tuning diagram:

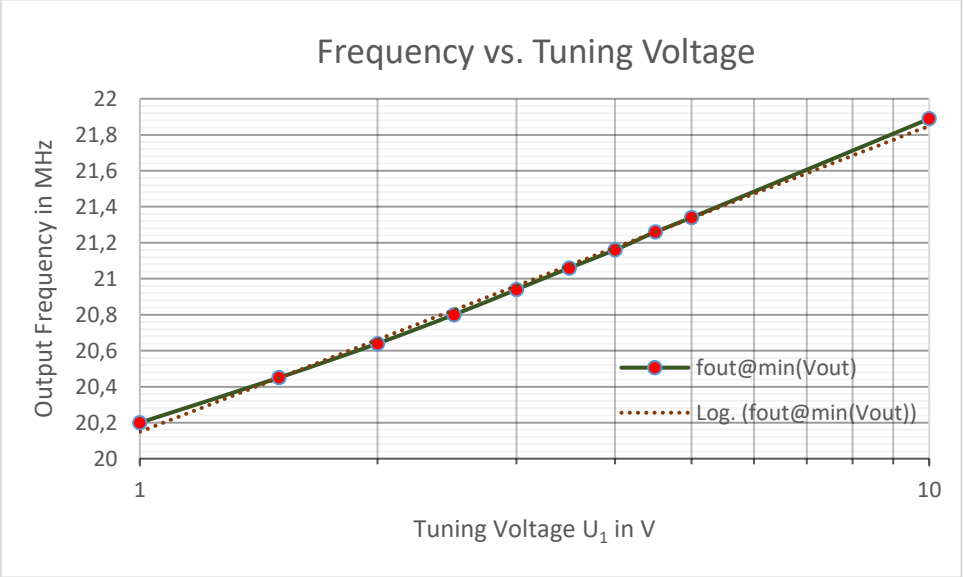

Figure 3.8: Dependence of the output frequency on the tuning voltages

The figure shows that the output frequency dependence on the tuning diodes is logarithmic with a small deviation from the ideal (dotted line). For DC voltages below the operating range of the diode ($U_{1,2} < 1V$), the performance is very bad: at this range it is not possible to adjust the minimum and the behavior is not logarithmic:

Table 3.4: Tuning range, measurement table

U_1	$f(V_{out,min})$	U_2	$P_{out}(U_1, U_2)$	$V_{out,min}(U_1,U_2)$
in mV	**in MHz**	**in mV**	**in dBm**	**in µV**
0	19,33	0	-48	1258,9
0,5	19,85	0	-59	363,1
1	20,20	35,2	-82	25,1
1,5	20,45	132,4	-84	20,0
2	20,64	215,7	-84	20,0
2,5	20,80	289,7	-85	17,8
3	20,94	363,2	-86	15,8
3,5	21,06	424,5	-86	15,8
4	21,16	481,2	-87	14,1
4,5	21,26	536,6	-84	20,0
5	21,34	594,7	-85	17,8
10	21,89	956,4	-85	17,8

Note: The minima are in very low voltage range where they can be detected by the spectral analyzer but not by a microcontroller. The definition of the minimum voltage depends on the resolution of the ADC. (section 4)

3.4. Output Load

The last simulation concerning the notch circuit is to evaluate the behavior of the circuits output under different load conditions. A parameter sweep is carried out to investigate the impact of different load resistors.

AC sweep, magnitude response:

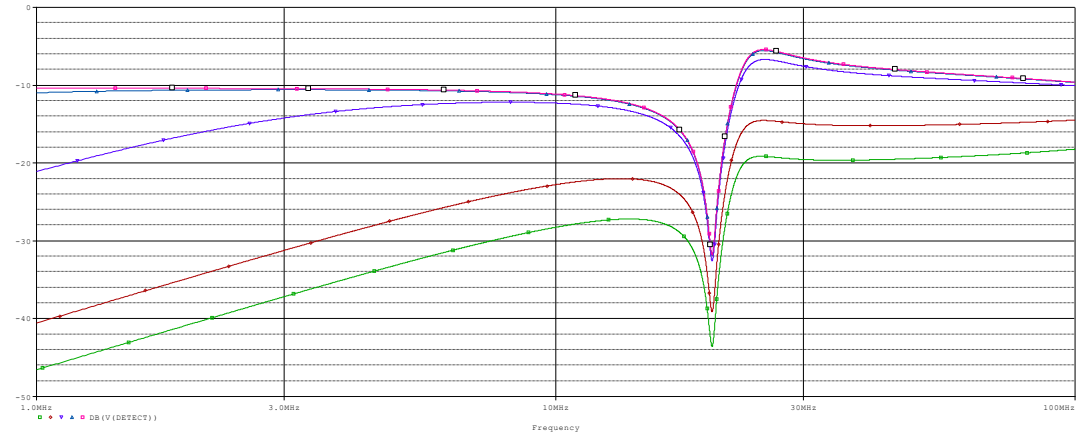

Figure 3.9: Parameter sweep of load resistor

The output frequency is stable while the amplitude is decreases for increasing load currents. A source follower must be implemented at the output to react on this observation. Its input in high-ohmic and its output enables a low-ohmic load to be connected to the circuit. The green response corresponds to $R_L = 50\Omega$, followed by 100Ω, 1kΩ, 10kΩ and the pink curve on top corresponds to $R_L = 1M\Omega$.

AC sweep, magnitude response:

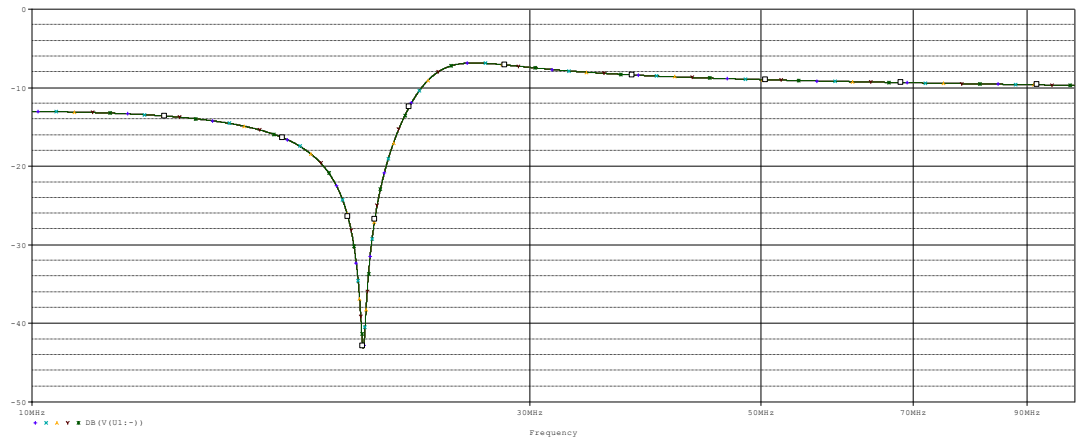

Figure 3.10 Parameter sweep of load resistor with output source follower

The simulation profile remains unchanged. The resistor values are the same as for figure 3.9. The result is as expected. The output of the circuit can be connected to the ADC without affecting the functionality of the circuit.

4. Signal Processing

The concept of undersampling is one possibility to replace the analog mixing stage of the original Denoth meter where extra crystal oscillators need to be implemented. A new design must include only a single high frequency crystal that will be attached to the microcontroller. Nevertheless, the signals of the analog circuit must be designed to feed the sensor and the ADC of microcontroller with appropriate voltage levels.

4.1. Source Signal

The source signal for the sensor circuit is a 20MHz sine wave. To have this signal available, the source signal must be processed between the microcontroller and the notch to have a good input signal for the sensor.

4.1.1. Generation of a Square Wave

The signal source is the microcontroller which generates a 20MHz square wave. The MSP430F6659 runs at this frequency. It is not possible to use a timer to generate a PWM output signal ($f_{max} = 10MHz$), but the subsystem master clock of the controller can directly be connected to pin 3.4 as peripheral function. The SMCLK can be sourced internally from different clock sources such as the DCO or the DCODIVCLK, the REFO clock or the VLO. It can be sourced externally with a high frequency crystal at the XT2 clock input pins. The VLO and the REFO clock are intended for low frequencies such as 10kHz and 32,768kHz respectively.

To find the right clock source, the digital controlled oscillator and an external source are compared to each other. By default, the DCO runs at a frequency of 1,045Mhz but it can be accelerated internally with a frequency locked loop and the REFO clock as reference. The drawback of this technique is that the generated clock frequency is not very accurate. A lot of jitter is introduced to the signal as well.

The other possibility is to use an external quartz. The MSP430TZ100USB evaluation board is equipped with a 2-pin crystal LFXTAL057056R250 in a HC-49 package from the manufacturer IQD. It operates according to the industry standard in a temperature range from -40°C to 85°C. It vibrates on the fundamental with a minimum frequency stability of ±30ppm. It requires a load capacitance of 12pF. The external capacitors must be calculated with respect to the parasitic capacitance of the microcontroller input pins and traces which is $C_{Parasitic} = 2pF$ [7].

The load capacitors C_{L1} and C_{L2} must be calculated correctly otherwise the vibration will deviate from the desired frequency. They produce, together with the crystal's inductance, the 180° phase shift for the feedback path.

The capacitors are connected in series through ground, thus for the crystal the load capacitance is:

$$C_L = \frac{C_{L1} \cdot C_{L2}}{C_{L1} + C_{L2}} \tag{4.1}$$

where for each capacitor C_L, the parasitic capacitance has to be added. Due to symmetry, equal capacitors must be used.

$$C_L = \frac{C_{L1} + C_{Parasitic}}{2} \tag{4.2}$$

Rearranging this equation yields for C_{L2} and C_{L2}:

$$C_{L1} = C_{L2} = (2 \cdot C_L) - C_{Parasitic} = 22pF \tag{4.3}$$

Clock frequency output:

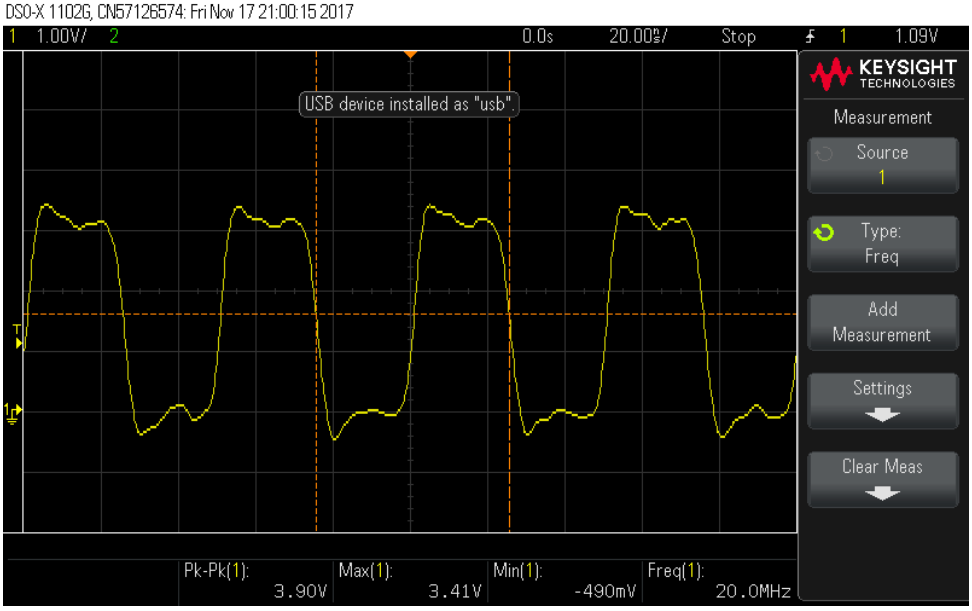

Figure 4.1: 20MHz source signal, measured with the oscilloscope at pin 3.2 of the MSP430F6659

The frequency is now stable enough to be converted into a 20MHz sine wave to source the sensor circuit. The square wave is filtered with passive LC structure of higher order to separate the overtones from the fundamental.

4.1.2. Filtering the Fundamental

A passive lowpass filter of 7th order is designed according to the guidelines for a 1dB-Chebyshev filter characteristic [8].

OrCAD Capture schematic:

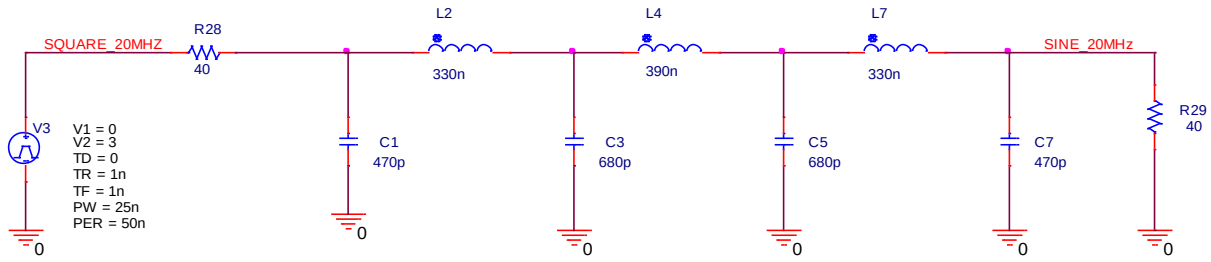

Figure 4.2: 7th order 1dB-Chebychev LC tank

The reason to choose this characteristic is that a steeper roll-off can be achieved than with a Butterworth or Bessel filter. Passband ripple is accepted because it is not affecting any functionality.

The digital output pin of the MSP430 has an output resistance of $R_{OUT} = 40\Omega$. It must be matched with the source resistance of the LC filter. The termination resistance of the circuit is equal to the source resistance. Coincidently, a signal loss of -6dB must be accepted because of the voltage divider. The normalized filter coefficients are taken from a look-up table [8]. The nominal element values are subsequently calculated with a MATLAB script.

The denormalizing factors are $\omega' = 1\,rad/s$ and $R' = 1\Omega$.

The frequency scaling factor is:

$$FSF = \frac{2\pi f_c}{w'} \tag{4.4}$$

The elementwise calculation is

$$R_S = R_L = \frac{Z_0}{R'} \tag{4.5}$$

$$L = \frac{L' \cdot Z_0}{FSF} \tag{4.6}$$

$$C = \frac{C'}{FSF \cdot Z_0} \tag{4.7}$$

Table 4.1: Element values for 1dB-Chebychev filter for a corner frequency of f_c=20MHz

Component	Normalized	Denormalized	Nominal
R_{SOURCE}	---	40Ω	39Ω, 43Ω
$R_{TERMINATION}$	---	40Ω	39Ω, 43Ω
C1, C7	2,2043	438pF	470pF
C3, C5	3,1472	626pF	680pF
L2, L6	1,1311	360nH	330nH
L4	1,1942	380nH	390nH

The resistors and capacitors have a tolerance of 1% in 0603 packages. The tolerance of the inductors is 30% within a 1008 package.

AC simulation, frequency sweep:

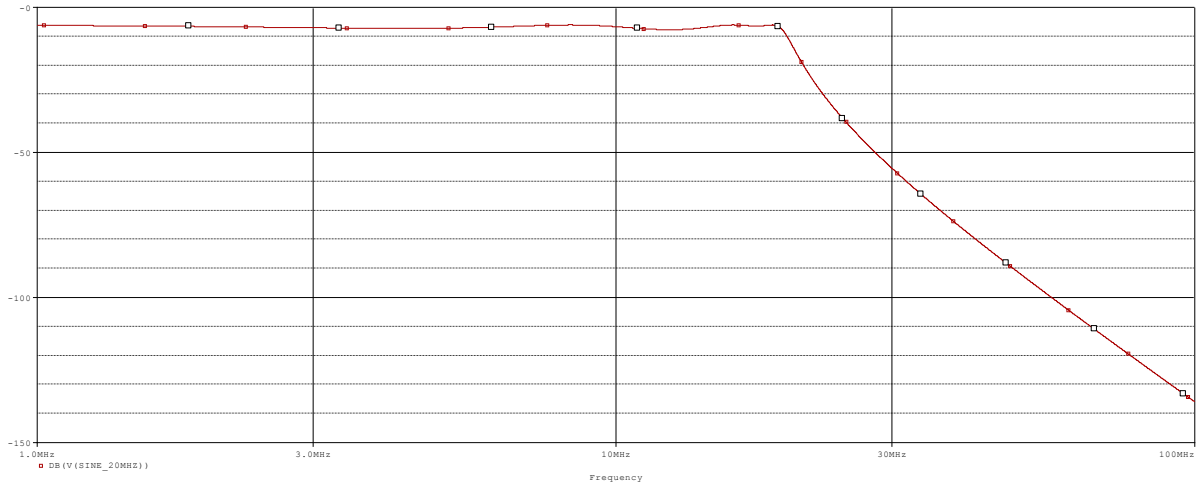

Figure 4.3: Frequency response of the Chebychev filter

The -3dB corner frequency is at $f_C = 19{,}6MHz$. The passband, measured at $18{,}6MHz$, is attenuated by $-6{,}06dB$ as expected.

The frequency of interest $f_{sig} = 20MHz$ attenuates by $-11{,}9dB$ due to the steep slope of the filter. The slope is measured from $-19{,}62MHz$ to $196{,}2MHz$, the value is $-168dB$ per decade which is more than expected.

The most interesting measurement concerns the frequency of the first overtone which is $40MHz$. The value is $-77dB$. This corresponds to a voltage value in the microvolt range.

Time domain simulation:

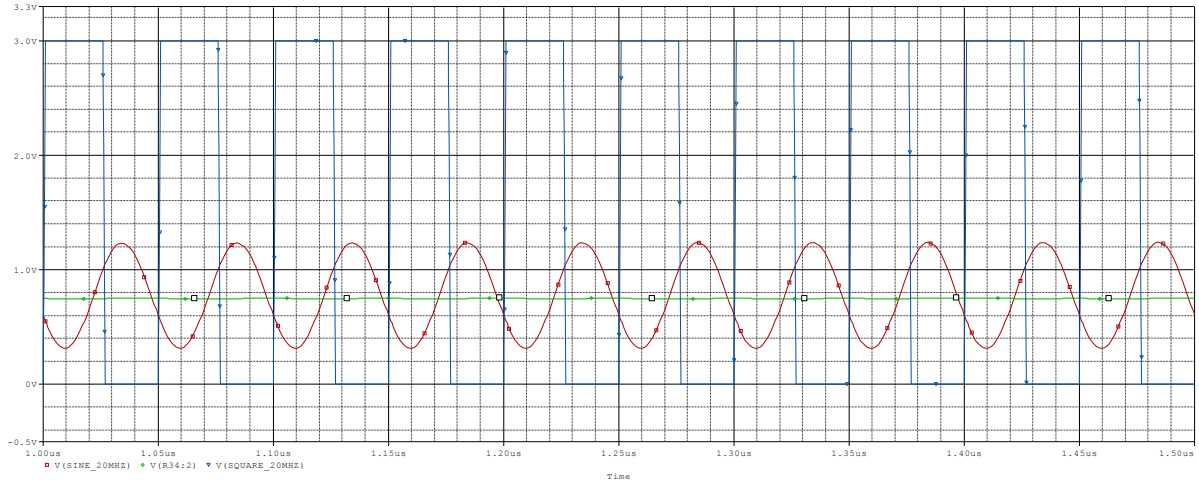

Figure 4.4: 7th order Chebychev filter (Input and Output signals)

The blue square wave is the model of the filter's input signal which behaves as the digital pin of the microcontroller that outputs the clock signal with 20MHz. The green signal is the simulation of a 40MHz sinewave which is filtered almost completely out.

The red signal is the attenuated fundamental wave. Its amplitude is 930mVpp. The DC offset is only half at 750mV because of the source/termination voltage divider.

Laboratory measurement:

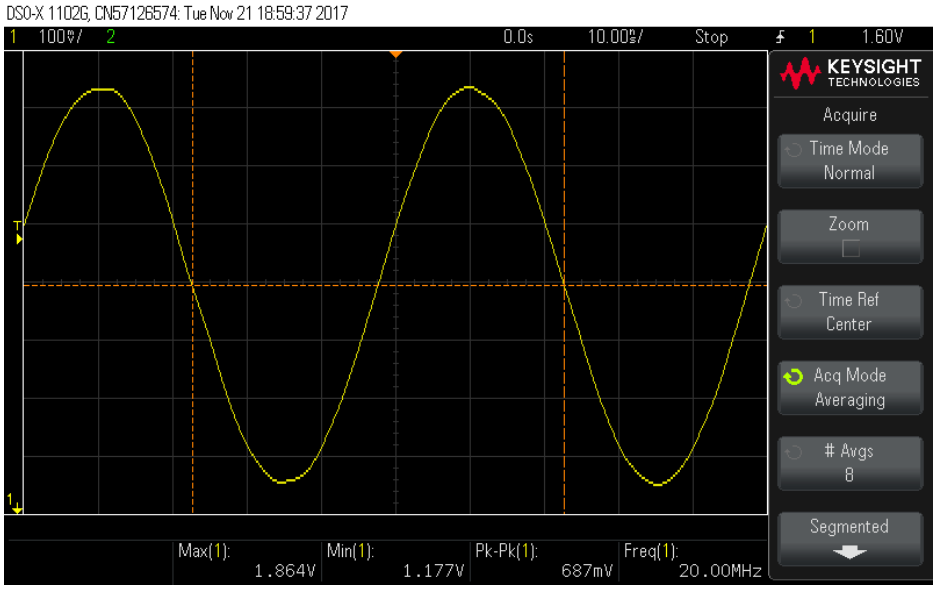

Figure 4.5: 20MHz fundamental wave

Figure 4.5 shows the time domain measurement of the filtered fundamental wave at the output of the LC tank. The offset V_{DC}=1,52V higher than with the simulation because different source resistor implementations in the simulation and lab setup. This DC offset is decoupled in the next stage anyway. The amplitude with $V_{OUT} = 680mV$ is somehow lower than expected.

4.1.3. Amplification

The amplifier stage is to ensure an appropriate signal amplitude plus an appropriate offset for the notch filter. The output of the Chebychev filter is kept at 40Ω. A capacitor (C_{31}) decouples the DC voltage. Right after this capacitor, a high ohmic voltage divider is connected to V_{CC} to bias the OpAmp correctly. The bias is set to 1,1V with the voltage divider (R_{24}, R_{25}) shown in figure 4.6.

Spice schematic:

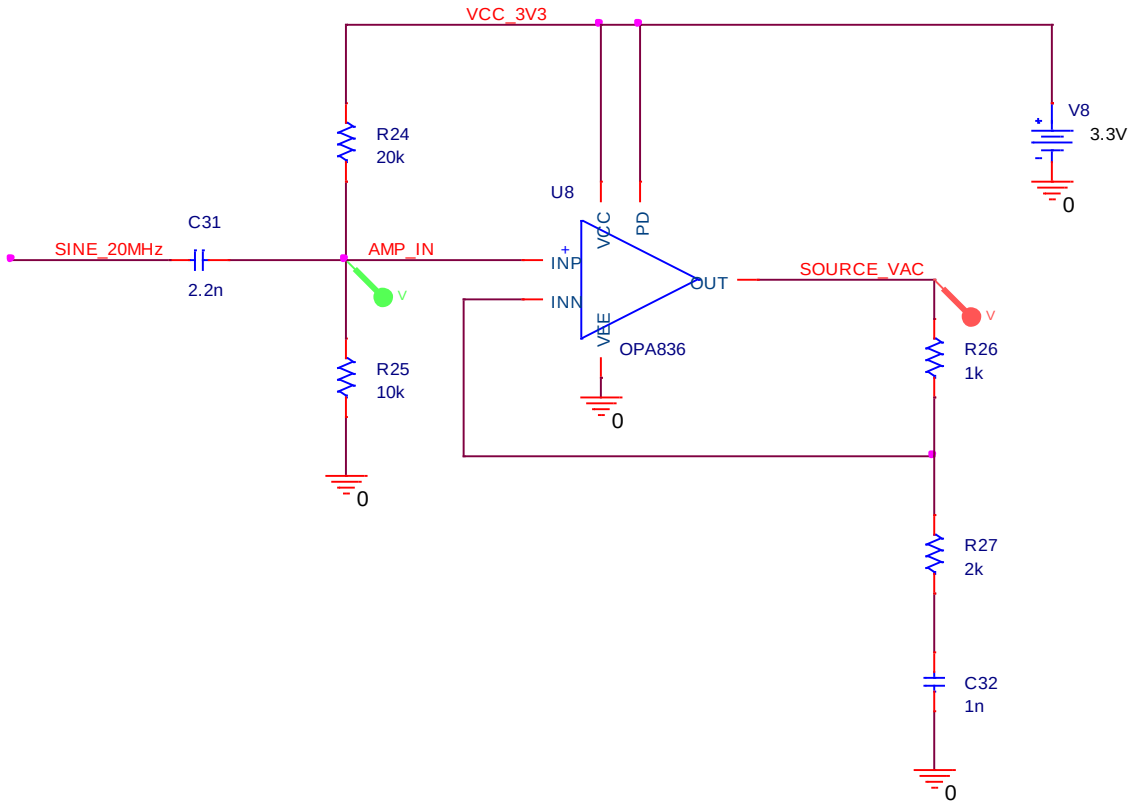

Figure 4.6: Non-inverting AC amplifier (DC follower configuration)

The OPA836 operational amplifier from Texas Instruments is implemented because of its high gain bandwidth of $GBW = 205MHz$, its very high slew rate $SR = 560\frac{V}{\mu s}$ and the temperature range from -40°C to 85°C. The output is rail-to-rail but the input stage unfortunately not. The datasheet guarantees a common mode input range from -0,2V to 1,6V with a power supply of 2,7V and up to 3,9V with a 5V supply voltage.

The feedback path indicates that the amplifier is operated as a DC follower in the non-inverting mode.

Amplification:

$$A_V = 1 + \frac{1k}{2k} = 1{,}5 \tag{4.8}$$

The bandwidth of the amplifier $B = \frac{205}{1.5} = 136{,}6$ is more than 12 times bigger than the frequency of interest. The magnitude response for the lowpass

$$H(f) = \frac{1}{\sqrt{1 + \left(\frac{f_S}{f_B}\right)^2}} = \frac{1}{\sqrt{1 + \left(\frac{20}{136{,}6}\right)^2}} = 0{,}98 \tag{4.9}$$

gives a satisfactory result.

The 2kΩ resistor and the capacitor form a high pass filter. The minimum size of the capacitor is calculated with respect to the $-3dB$ corner frequency at $f_c = 20MHz$.

$$C_{32} = \frac{1}{2\pi R_{27} f_c} > 400pF \tag{4.10}$$

To ensure that the signal will not be attenuated, the capacitor is dimensioned with $1nF$.

Also the input capacitance C_{31} forms a highpass with the voltage divider resistors R_{24} and R_{25} (AC-wise in parallel). The calculation yields a minimum capacitance value with $1{,}2pF$. The implemented capacitor with $C_{31} = 2{,}2nF$ is much bigger than the minimum because of the best transient behavior observed during simulation.

Figure 4.7 shows the simulated signals at the amplifier stage. The green signal is the input signal, measured at AMP_IN (figure 4.6). The red curve describes the output signal which drives the sensor circuit, measured at SOURCE_VAC. Both signals have a DC offset of 1,1V. The amplitude of the output signal $is\ V_{OUT} = 1{,}4V_{pp}$.

Time domain simulation of the input and output signal at the amplifier stage:

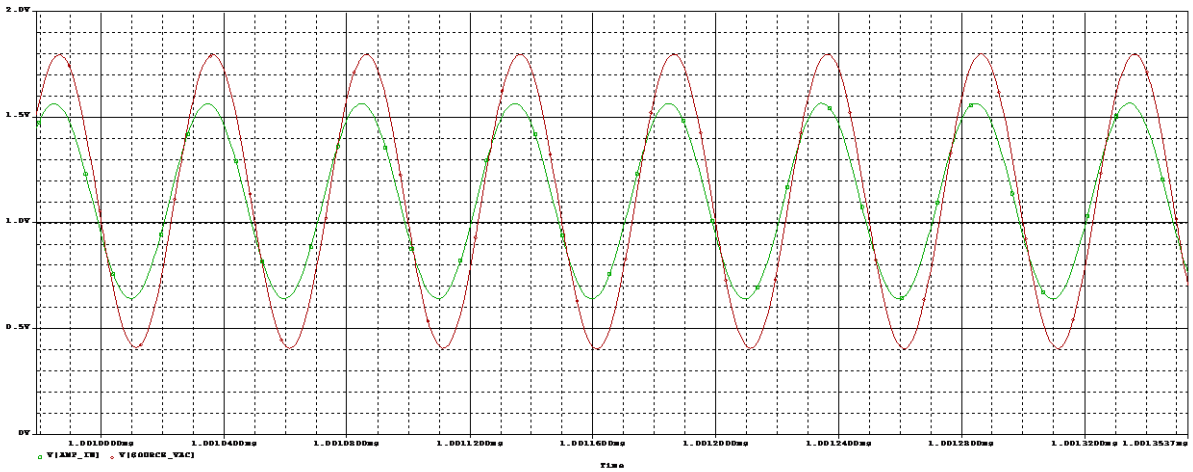

Figure 4.7: Input and output signal of the amplifier stage

4.1.4. Laboratory Measurements

The sensor circuit is built on an evaluation PCB. The filter is fed with a 20MHz square wave signal from a 50Ω source and the output is measured. The source and termination resistors are substituted by 50Ω coax cables (SMA) to maintain signal integrity. The bill of materials can be looked up in table B.2.

Altium, 3D-view:

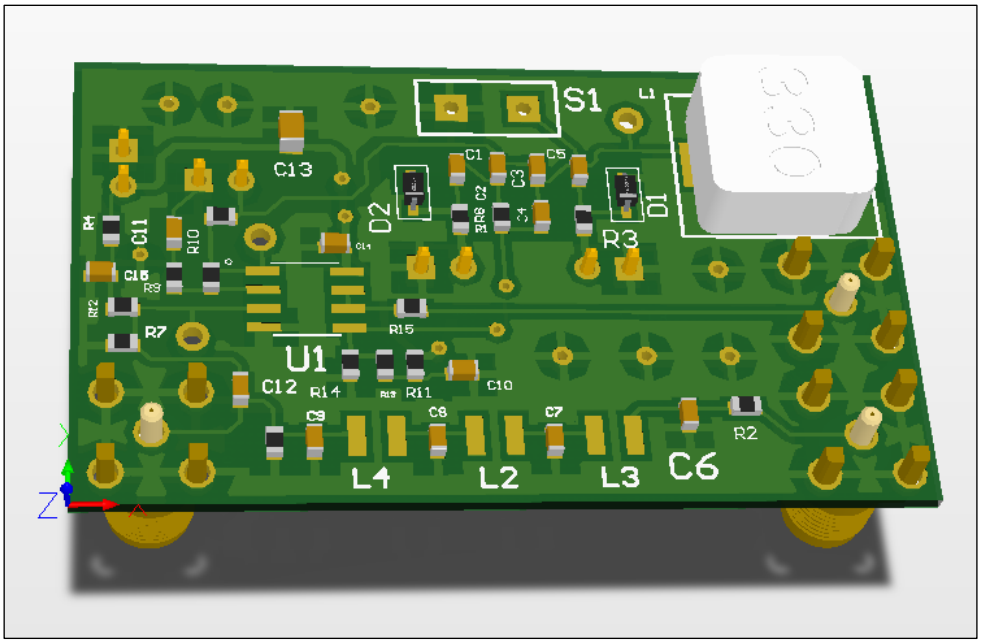

Figure 4.8: Sensor circuit prototype PCB

The frequency response of the real implementation of the LC filter is similar to the simulation result (compare figure 4.3 and figure A.7). The frequency of interest at 20MHz is attenuated

by -10,56dB, the 2nd harmonic at 40MHz is attenuated by -72dB, the 3rd, 4th and 5th by almost -80dB. These results are obtained with a frequency sweep by the spectral analyzer.

The next figure shows the spectrum when the LC filter is sourced by the microcontroller with the 20MHz clock signal.

Spectrum:

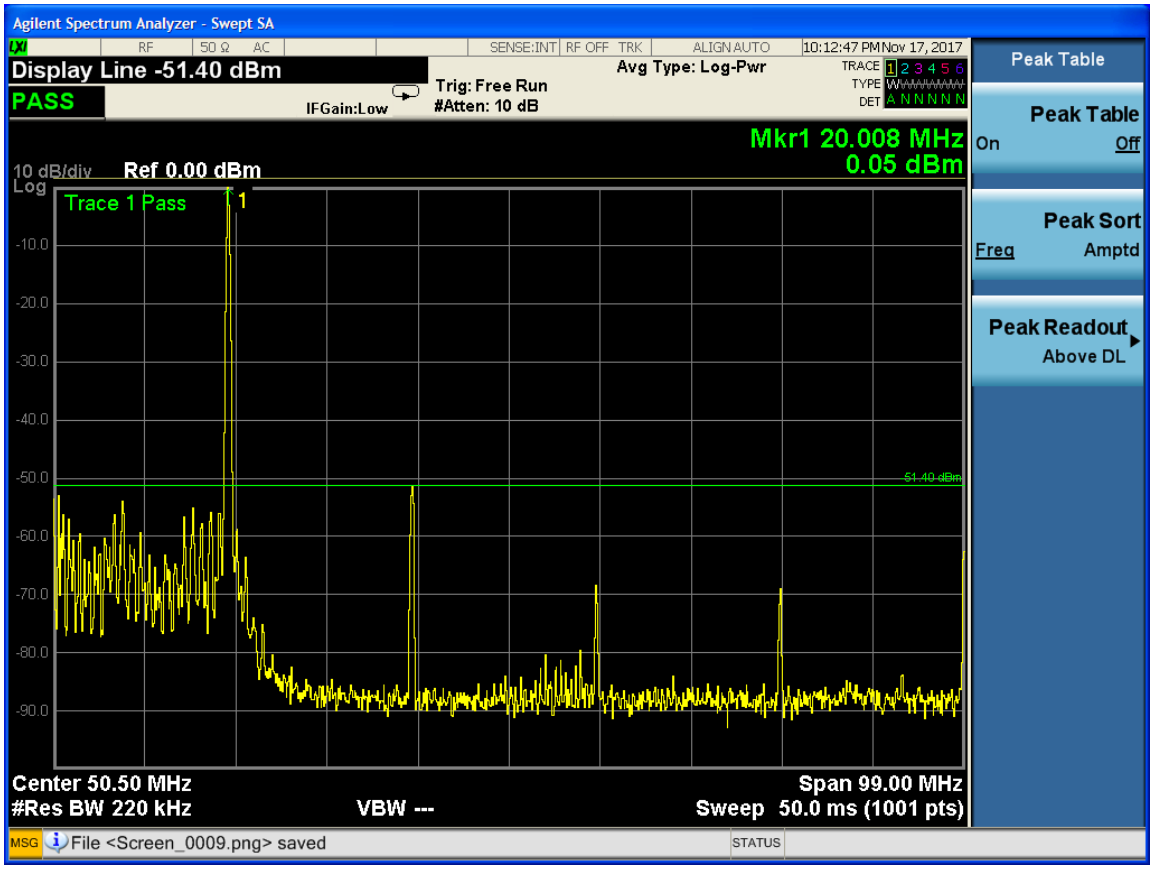

Figure 4.9: Spectrum of the filtered input signal

The 20MHz signal has a power of $P = 1mW$ at the output of the input signal filter stage. The 2nd harmonic at 40MHz is attenuated by -51,4dBm, the 3rd, 4th and 5th are close to the noise floor.

The operational amplifier is supplied by the microcontroller with 3,3V. The time domain signals at the input and output of the amplifier are measured with the oscilloscope.

Transient measurement:

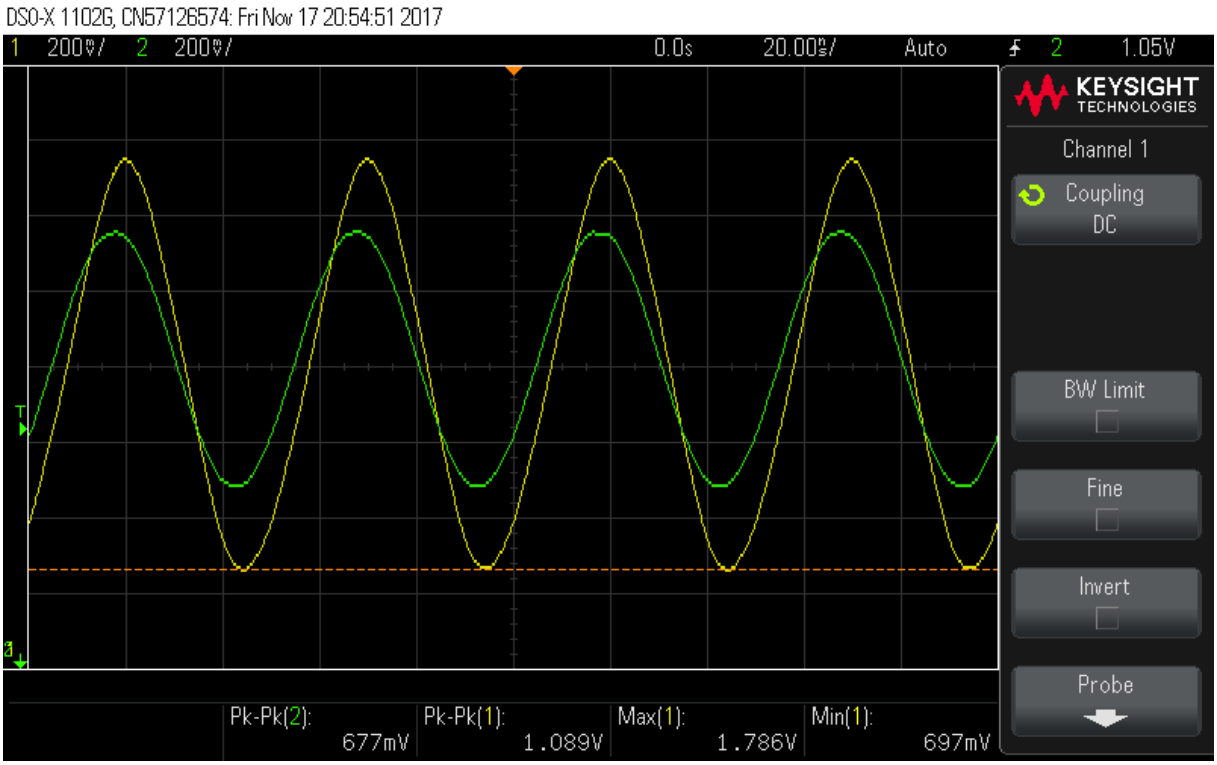

Figure 4.10: Input and output signal at the amplifier stage

The frequency measurement of the input and output signal gives $f = 20{,}0MHz$ (figure A10). The supply voltage sourced by the microcontroller and the DC offset at the positive input of the single-supplied amplifier are measured with a multimeter at $V_{CC} = 3{,}084V$ and $V_{DC} = 1V$, respectively. The amplification $A_V = 1{,}6$ is calculated with the measured results and accepted as adequate.

4.2. Signal Detection: Analog Part

The most challenging task for this project is to handle the output signal of the notch filter because it is a minimum that is expected to be in the low millivolt range.

4.2.1. Simulation

The same simulation setup as in section 3.1 is used to evaluate the signal amplitude.

AC sweep:

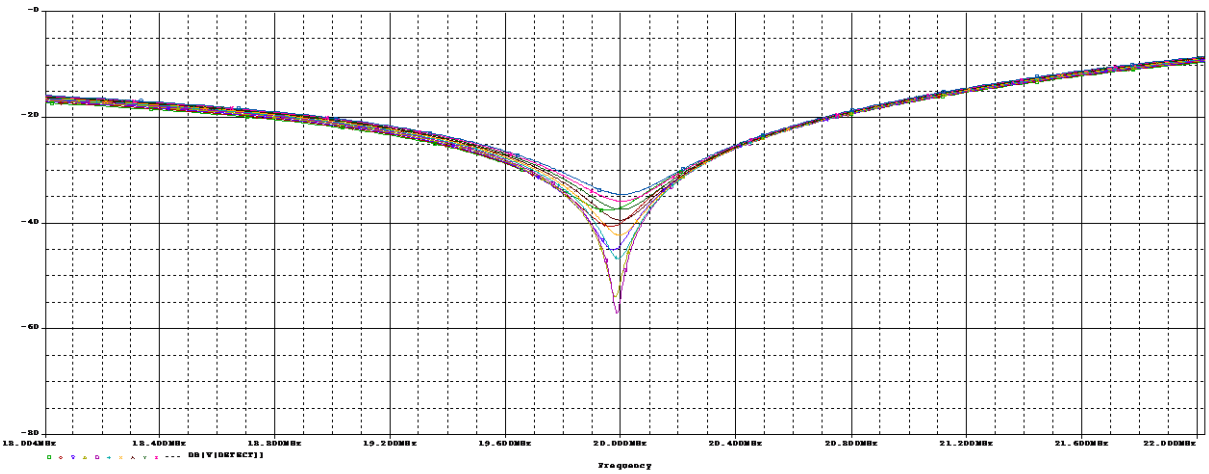

Figure 4.11: Minimum signal detection

To find the minimum of the current setup with

- $\varepsilon' = 1 \rightarrow C_{Sens} = 1pF$
- $V_{D1} = 1V$

V_{D1} is swept from 1V to 2V. The DC voltage of this minimum is at $V_{D2} = 1{,}8V$.

Time domain simulation with the tuning voltage from above:

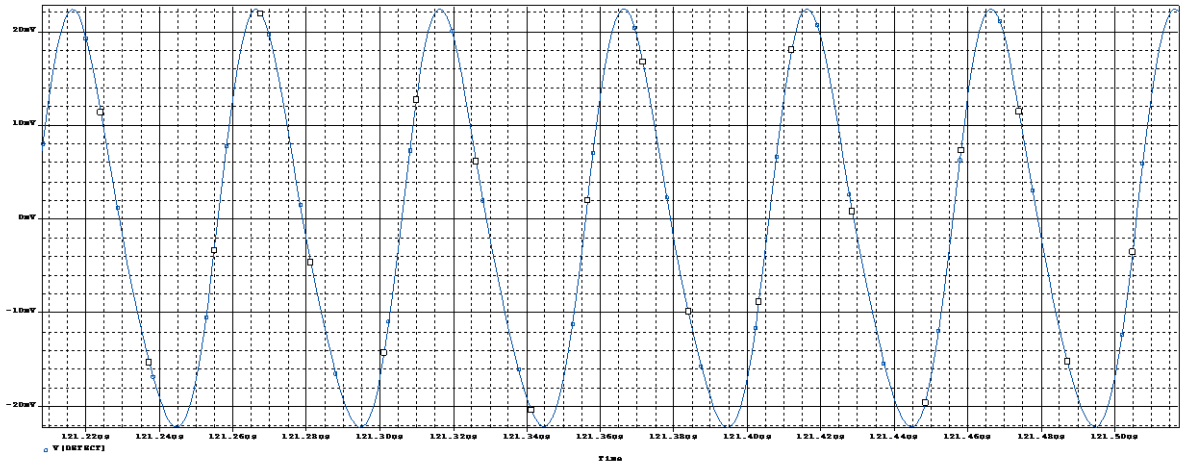

Figure 4.12: Output signal of the sensor circuit

Figure 4.12 shows the minimum signal which has been adjusted with the tuning voltage of the resonance circuit. The sensor was simulated exposed to air. The amplitude is measured with $V_{Detect} = 44{,}7mV$, peak-to-peak. One has to note that the output is not a perfect sine wave.

Some different ideas have been considered to detect such a small voltage with a microcontroller.

The first Idea concerns the on-chip ADC of the microcontroller. The MSP430F6659 is equipped with SAR ADCs with 10bit and 12bit resolution respectively. The smallest change in the analog voltage that yields a change in the digital output is:

$$\Delta V = \frac{V_{ref}}{2^N} \tag{4.11}$$

where N describes the number of bits. The internal bandgap reference of the currently used MSP430 can be adjusted to 1,5V, 2V or 2,5V. Since ΔV should be as small as possible to achieve the maximum resolution, the voltage is set to $V_{REF} = 1{,}5V$.

12 bits correspond to 4096 different values. One bit must be reserved for the negative sign because the signal will be expressed as two's complement. Hence, 2048 values are available to describe the 22mV minimum amplitude of the sensor circuit's output.

According to equation 4.11, 1 LSB represents $\Delta V = 730\mu V$.

The Spice simulation tells that a 12bit ADC would be sufficient to detect the minimum. If one evaluates the following picture which was obtained with the oscilloscope in a laboratory experiment and the prototype circuit, the simulation result seems to be not accurate enough.

Different minima in a series of test setups have been recorded at the lab, such as the example in figure A12. The minimum is at -58,3dB.

This corresponds to a voltage of approximately

$$V = \sqrt{P \cdot R} = \sqrt{10^{-9}W \cdot 50\Omega} = 220\mu V \quad \Rightarrow \quad V_{PP} = 622\mu V \tag{4.12}$$

In this case, the resolution of the 12bit ADC is too less.

Alternatives with ADCs would be:

- MSP430 controller which is equipped with the 24bit ΣΔ-ADC to have a much higher resolution. The sampling rate may be reduced, but sufficiently high to accomplish the method of Undersampling which is intended to be used in this project. A high SNR should be achieved with noise.
- Amplifying the signal that the level of the minimum is high enough to be resolved by the ADC. It must be accepted that the signal will be clipped, if the output voltage is higher than for the minimum case.
- Connect external ADC's to achieve 16bit, 18 bit or even higher resolutions.

Another idea is to use a logarithmic amplifier to translate the minimum into a DC voltage which could be easily detected by the microcontroller. The RSSI function of a LogAmp is designed to detect input signals over a huge range and a very large bandwidth. The AD8309 would be such a device with a dynamic range from -78dB to 22dB with a guaranteed linear measurement up to 200MHz. Also the temperature drift of the device is very low. Unfortunately, a Spice model could not be obtained to simulate the functionality of this device.

A third possibility would be to rectify the signal with an analog circuit, such as a precision rectifier circuit, and measure the resulting DC voltage with the microcontroller.

4.3. System Verification

The sensor circuit prototype is again connected to the spectral analyzer to confirm the principle of operation (equation 2.14). The sensor is substituted by capacitors of appropriate values to simulate a connected sensor exposed to material with different permittivity. The differential capacitance plus the backplane are implemented with a 22pF (nominal) capacitor. The following experiment is to simulate different permittivity values that are multiples of $\varepsilon_R' = 1$.

The input signal (50ms sweep) is generated by the RF source of the spectral analyzer. The output signal is measured at the source follower of the notch circuit.

Spectrum:

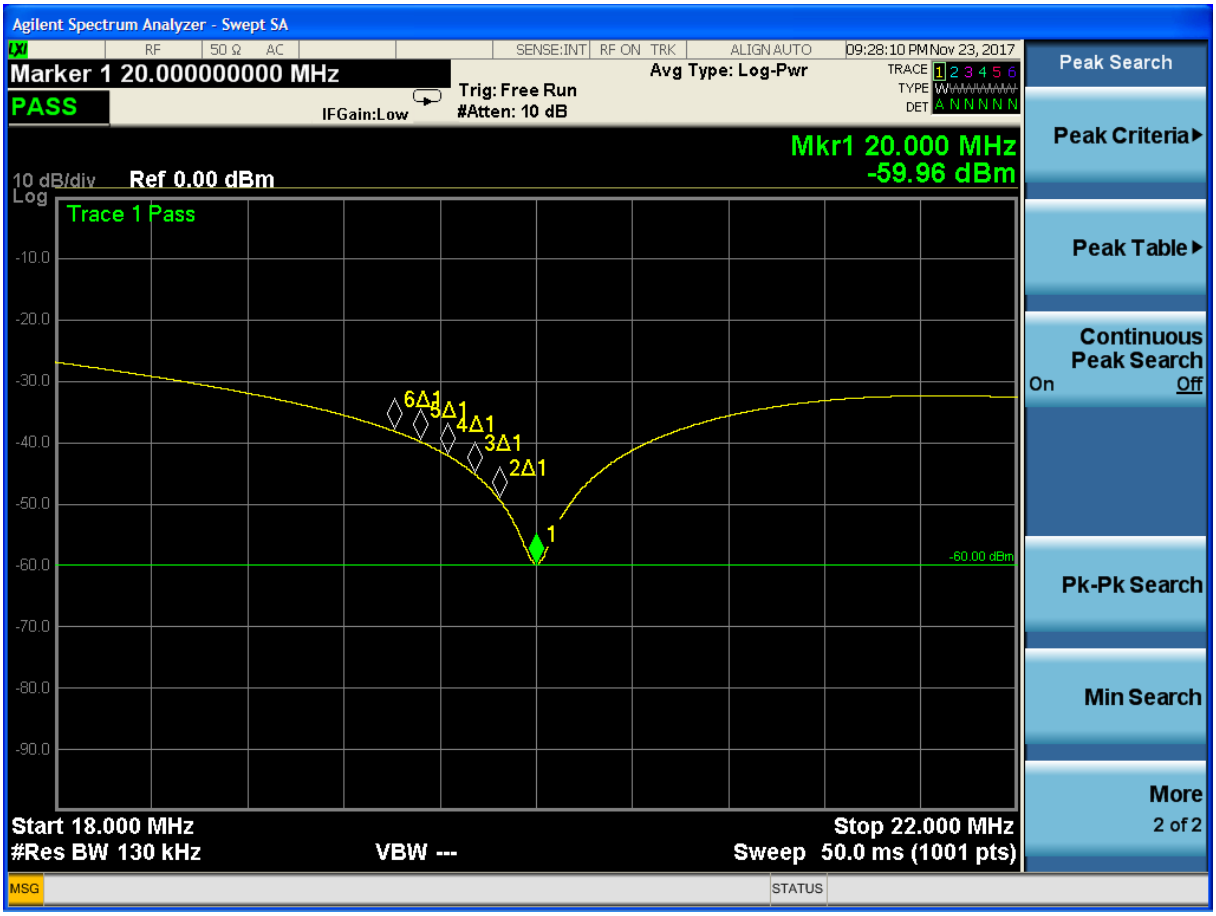

Figure 4.13: Spectrum of the prototype output signal

The markers are placed at the frequencies where the minimum drifts in case of an increased sensor capacitance in 1pF steps. The used capacitors have a tolerance of 25%. The capacitors are checked with the LCR brigde to determine their real capacitance. The spectrum and the capacitor measurements are evaluated and noted in table 4.2.

The following measurement procedure has been performed to verify the measurement and operation principle of the Denoth meter:

- Calibration with Air:

A capacitor with nominal 22pF was attached between the connector S1 and ground to simulate the sensor electrodes and the floating backplane. The sensor is determined to be 1pF, the backplane with nominal 21pF. It is essential to implement this 22pF because the elements of the circuit are dimensioned to operate at a frequency of 20MHz. If the sensor value is adapted to another reasonable value, e.g. 700fF, the result of this experiment will be the same if the formulas are applied correctly.

The sensor circuit is connected to the analyzer and the minimum is of the spectrum is tuned to 20MHz. The corresponding tuning voltage U_1 is noted as V_{REF}.

- Measurement:

Three different capacitors ($C_1 = 1{,}33pF, C_2 = 2{,}21pF, C_3 = 2{,}88pF$) in various combinations are soldered stepwise in parallel to the 22pF-capacitor ($C_B = 22{,}41pF$) to simulate multiples of the reference dielectric (air, $\varepsilon'_R = 1$). Voltage U_1 is tuned in such a way that the minimum is again at 20MHz, and is noted as V_M.

Voltage U_2 is tuned in a way, that the minimum is turned back to -60dBm to compensate the losses. Since there are no losses expected with these capacitors, the value of U_2 is expected to remain unchanged during the whole experiment.

- Computation:

The sensor specific constant k must be calculated initially: Therefore, one must consider equations 2.10 and 2.11.

$$k = \frac{a_2}{k_2} = \frac{\dfrac{\Delta C_{Diode}}{\log_{10}\left(\dfrac{V_{tuning1}}{V_{tuning2}}\right)}}{C_{Sensor}} = \frac{\dfrac{19{,}37pF - 15{,}78pF}{\log(2V) - \log(1V)}}{1pF} = 11{,}926 \tag{4.13}$$

It is necessary to determine the slope a_2 that is expressed by the change of the capacitance in the resonant circuit and the change of the tuning voltage for that range. Variable k_2 is the sensor capacitance.

In the next step, V_M and V_{REF} are inserted in equation 2.14. The result for the relative permittivity ε'_R can be calculated.

Table 4.2: Cursor measurements at figure 4.13

ΔC = Δε'	ΔC = Δε'	Δf	U_1	U_2	ε' (calculated)	ε' (expected)	Deviation	ε''
in pF (nom.)	in pF (meas.)	in kHz	in V	in mV	Equation 2.14	Equation 2.20	in %	
0	0	0	0,722	34,2	-	-	-	-
1	1,33	128	0,934	34,2	2,3327713	2,33	0,11	0
2	2,21	236	1,108	34,2	3,2171505	3,21	0,22	0
3	3,54	364	1,432	34,2	4,5450773	4,54	0,11	0
4	5,09	528	1,919	34,2	6,0604903	6,09	-0,48	0
5	6,42	628	2,286	34,2	6,9664252	7,42	-6,11	0

The experiment proves the good functionality of the sensor circuit and the operation and measurement principle to calculate the relative permittivity ε_R' of the Denoth meter. The accuracy up to a $\varepsilon_R' = 4{,}5$ is observed to be very good (Error < 0,22%).

The influence of losses in terms of accuracy cannot be tested with capacitors instead of the sensor. Therefore, well known lossy materials need to be tested in combination with the real sensor, and a calibration curve needs to be established.

Measurement result:

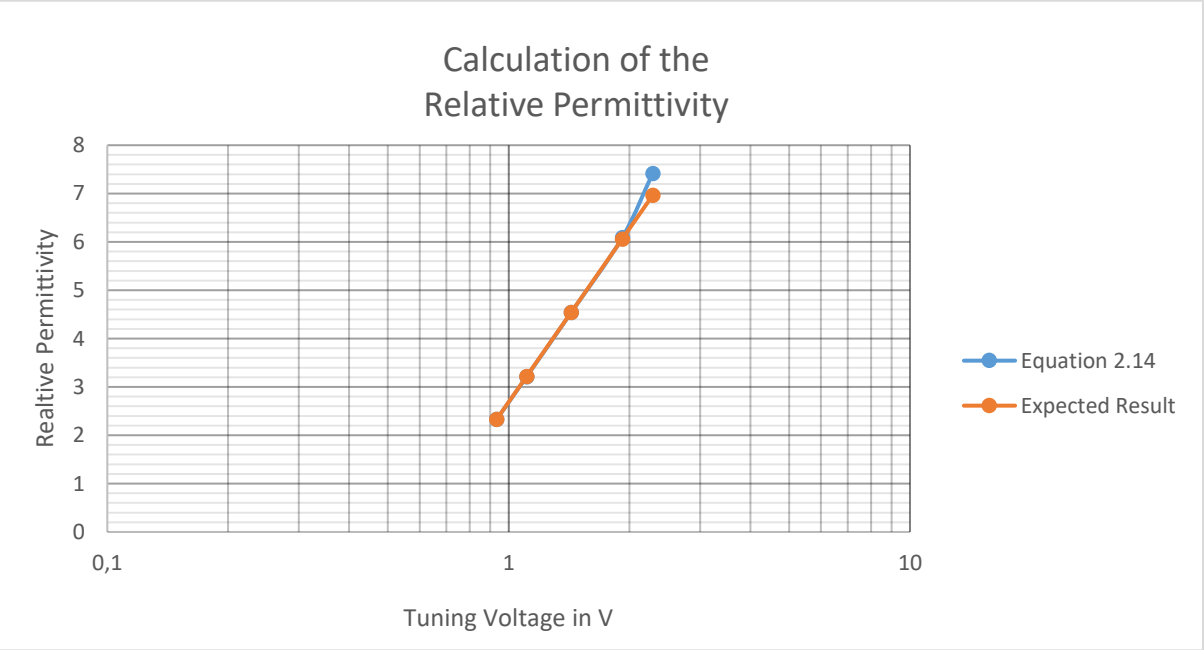

Figure 4.14: Calculation of the relative permittivity

Figure 4.14 shows the graphic representation of the measured and subsequently calculated results of table 4.2. The results are very much appreciated in terms of accuracy. Only for higher values of ε_R' (that is beyond the range of interest) significant deviations are observable.

4.4. Signal Detection: Digital Part

The concept of undersampling is to replace the analog mixing stages of the original Denoth meter to avoid inaccuracy due to temperature drift of the extra crystal. The minimum voltage should be detected by application and evaluation of an FFT.

4.4.1. Undersampling

The idea is to deliberately violate the Nyquist criterion in such a way that the sampled signal is assigned to a lower frequency without any information gets lost. This method is also referred to as digital mixing.

The MATLAB script with the exact (not rounded) values can be found in the appendix. Here, the explanation:

A frequency of $f_{signal} = 20MHz$ corresponds to a period of $T_{signal} = 50ns$.

The sampling frequency is not allowed to be a multiple of the frequency of interest because of aliasing. The maximum sampling rate of the currently used MSP ADC is 200kS/s. The undersampling rate is decided to be 190kS/s, hence, every $T_s = 5{,}26\mu s$ a sample is taken.

$$m = \frac{5{,}26 \cdot 10^{-6}}{50 \cdot 10^{-9}} = 105{,}26 \tag{4.14}$$

Every 105th period of the signal, a sample will be taken. 19 iterations are necessary when concatenating those periods to get a full period of the original signal.

$$f_{uss} = \frac{1}{Iterations \cdot T_s} = \frac{1}{19 \cdot 5{,}26 \cdot 10^{-6}} = 10kHz \tag{4.15}$$

The 12bit ADC is triggered by the CCR1 register of Timer A which is sourced internally by the DCO clock of the microcontroller and the REFGEN as explained in the previous section. The DCO is switched corrected to 1,9MHz, the compare register value is CCR1 = 5.

4.4.2. Fast Fourier Transform

After undersampling, the original signal of 20MHz is converted to 10kHz and can be processed by the FFT algorithm. The best result would be if the frequency of interest lies exactly on a frequency bin of the discrete FFT spectrum. If an integer number of periods is in the period of observation, this result will be achieved.

The following relation must be considered:

$$Number\ of\ Bins \cdot T_s = Number\ of\ Periods \cdot T_{uss} \tag{4.16}$$

With T_S as the sampling period and T_{USS} as the period of the undersampled signal.

$$N = \frac{1024 \cdot 5{,}26 \cdot 10^{-6}}{19 \cdot 5{,}26 \cdot 10^{-6}} = 53{,}9 \tag{4.17}$$

For the current implementation, 53,9 periods are in the period of observation T (acquisition time). The frequency of interest does not lie exactly on a bin. This issue should be resolved by evaluating the envelope of the discrete frequency values by zero padding. Hence, the resolution $\Delta f = \frac{1}{T} = \frac{f_S}{N}$ will be increased because the acquisition time is elongated.

An algorithm must be implemented that evaluates the FFT results to detect the voltage minimum of the sensor output.

5. Conclusion

This master thesis shows that a measurement of the dielectric constant with a capacitive sensor is possible. The real part of this complex quantity is obtained with good accuracy. For the imaginary part it is necessary to obtain a calibration curve with well-known materials or the method must be adapted. For the latter, a re-design of the sensor will be necessary.

The main part of this work covers the operating principle of the originally introduced Denoth sensor and the sensor circuit. The sensor is flat-plate PCB that allows to determine the change of the relative permittivity within a certain range. It operates at a frequency of 20MHz, that's why the relative permittivity must be considered as a complex quantity. The real part is related to the snow density, the imaginary part considers the water content.

The sensor is part of a tunable resonant circuit. Tuning is achieved with two varactor diodes. The original equation that was provided by the original paper has been derived, and has been evaluated with a laboratory experiment. It is based on the principle that the diode has a linear operating range for the logarithm of the tuning voltage which is verified for a range between 1V and 10V. The tuning voltages are used to calculate the real part of the relative permittivity and to determine the imaginary part by empirical relations. An alternative mode of calculation has been investigated additionally.

The computation of the snow density based on the relative permittivity has been covered theoretically and experimentally. It is considered to use a state-of-the art microcontroller which is capable of both, to source the circuit with the appropriate input signal and to detect the output signal.

The concept of an analog mixer close to the sensor electronics to be able to attach the sensor to a handheld unit is regarded as outdated and suggested to be replaced by the concept of undersampling. A Bluetooth module such as the RN-41 could be used instead of cables to connect the sensor to a mobile phone. The serial interface should be replaced by USB for a product development in the future.

6. Bibliography

[1] A. Denoth*: Snow Dielectric Measurements*

Advances in Space Research, Vol. 9, No. 1, pp. 233 – 243, 1989

[2] A. Denoth, A. Foglar: *Recent Developments of Snow Moisture Dielectric Devices*

Paper presented at ISSW 86, Lake Tahoe, CA, p.72, 1986

[3] John R. Kendra: *Snow Probe for In Situ Determination of Wetness and Density*

IEEE Transactions on Geoscience and Remote Sensing, Vol. 32, No. 6, 1994

[4] S. Sugiyama: *Dielectric Permittivity of Snow measured along the route traversed in the Japanese-Swedish Antarctic Expedition 2007/08*

Annals of Glaciology 51, 2010

[5] A. Denoth: *An Electronic Device for Long-term Snow Wetness Recording*

Annals of Glaciology 19, 1994

[6] H. Zumbahlen: *Basic Linear Design Handbook*

Chapter 8: Analog Filters, Analog Devices, 2007

[7] R. Okorn: *General Electrical Engineering III*

Lecture Notes, 2.6.7 Quasi-stationary fields in cylindrical conductors, Ref. 1.4, p. 50, 2006

[8] A. Williams: *Analog Filter and Circuit Design Handbook*

Chapter 3: Low-Pass Filter Design, McGraw-Hill Education, 2014

7. Appendix

A. Supplementary Figures

A.1. Sensor Geometry and Dimensions

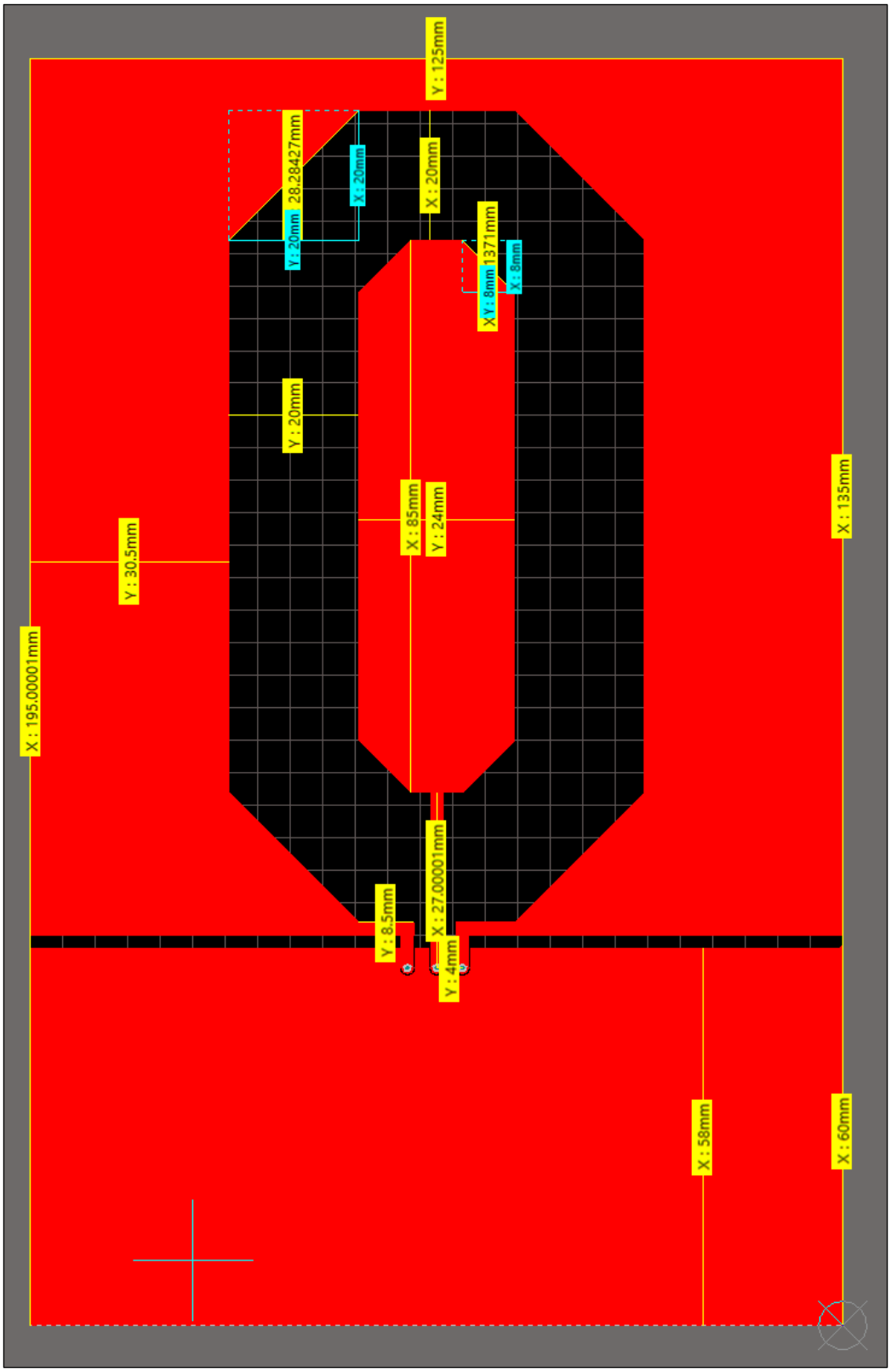

Figure A1: Geometry and dimensions of the Denoth sensor (top) with extra space for the sensor circuit, the microcontroller circuit, the Bluetooth module and a battery pack (bottom area).

A.2. Sensor Capacitance Measurements

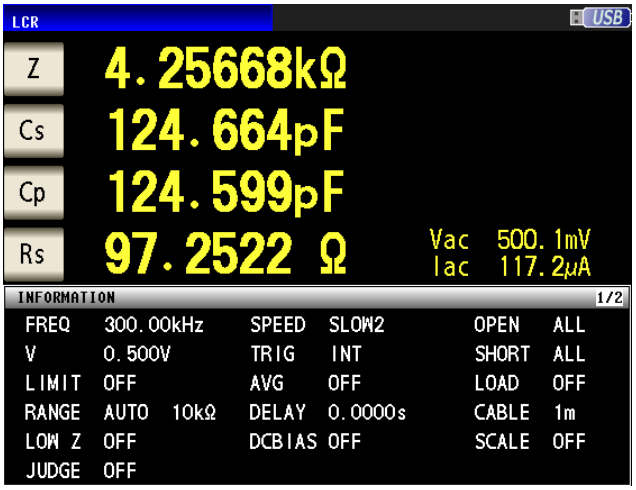

Figure A2.1: Capacitance between outer electrode and backplane

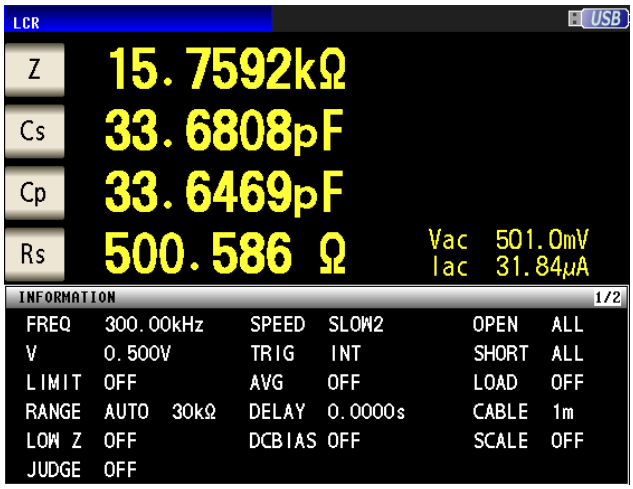

Figure A2.2: Capacitance between inner electrode and backplane

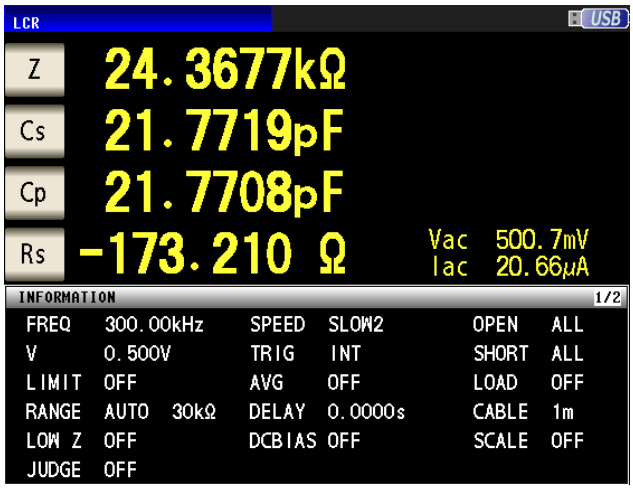

Figure A2.3: Differential measurement of the sensor capacitance 2 with a floating backplane

A.3. Impedance Measurement Results with Different Dielectric Materials

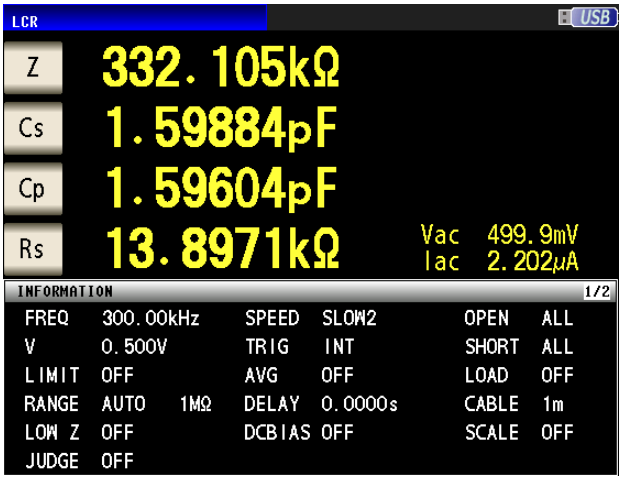

Figure A3.1: Sensor exposed to unknown type of plastic

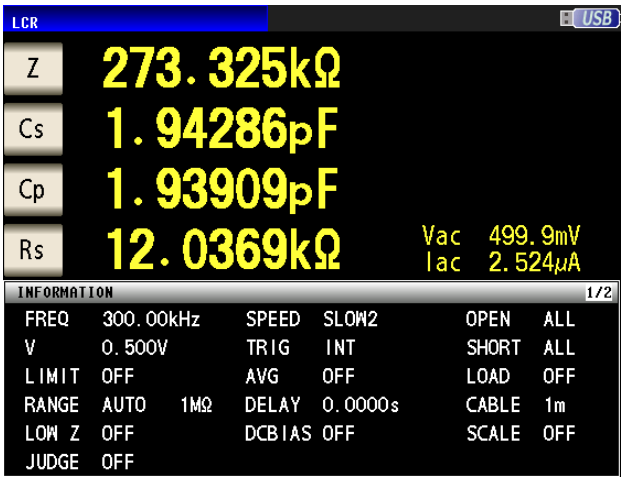

Figure A3.2: Sensor exposed to plywood

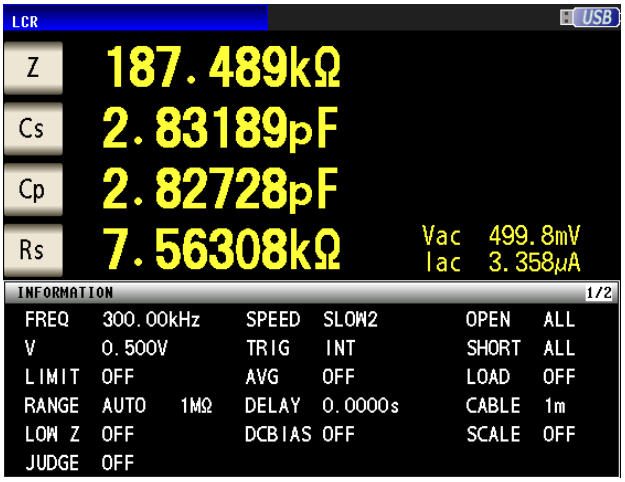

Figure A3.4: Sensor exposed to varnished wood

A.4. Bandstop Filter Characteristics

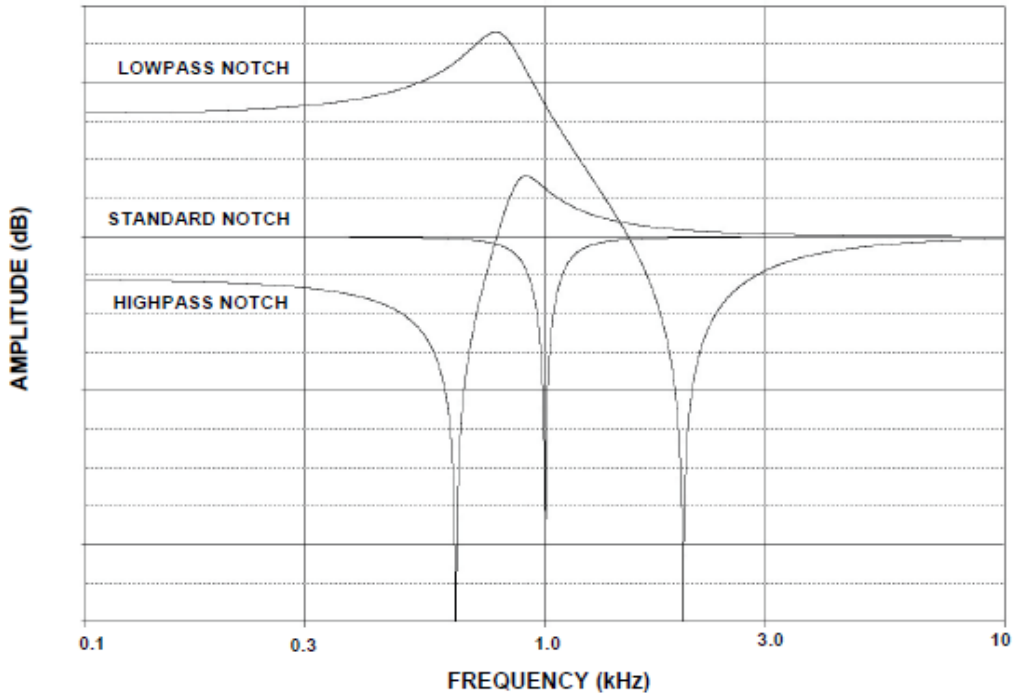

Figure A4: Standard, lowpass and highpass notch [6]

A.5. HF-Probe Measurement

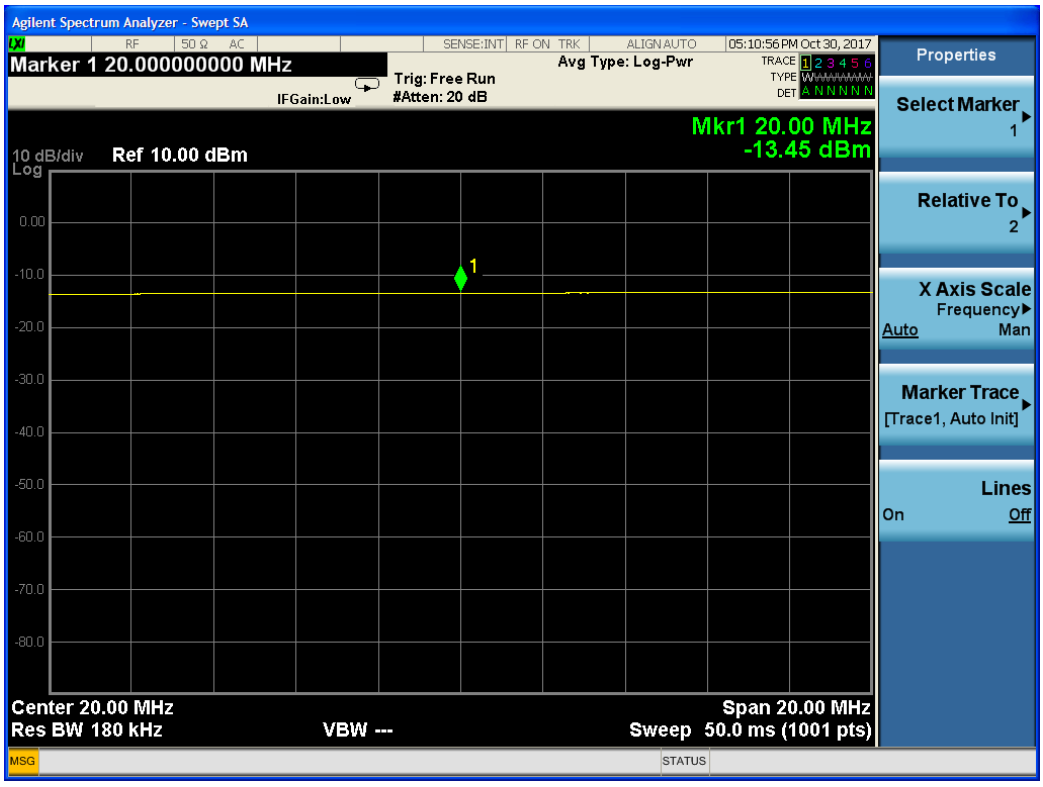

Figure A5: Attenuation of the Hewlett Packard high frequency probe

A.6. Influence of the Backplane on the Calibration Process

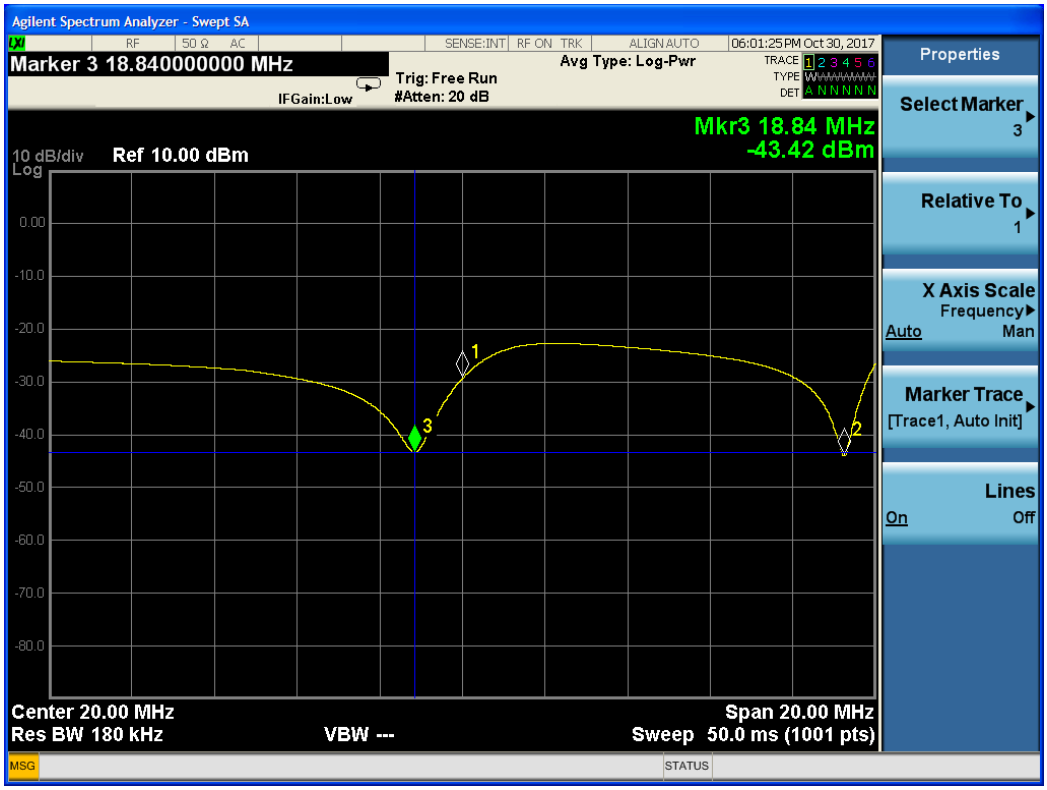

Figure A6.: Air calibration process (backplane connected to outer electrode)

A.7. Frequency Response of the LC filter

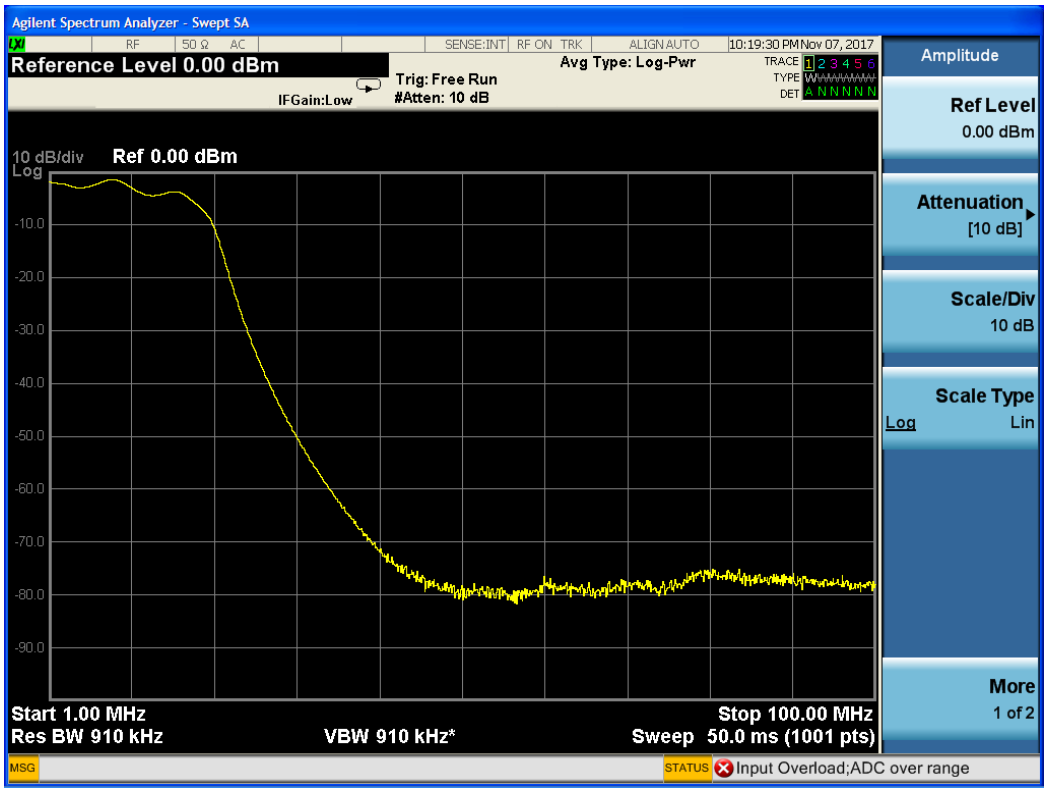

Figure A7: Magnitude response of the Chebychev filter

A.8. Sensor Circuit Prototype PCB (Top)

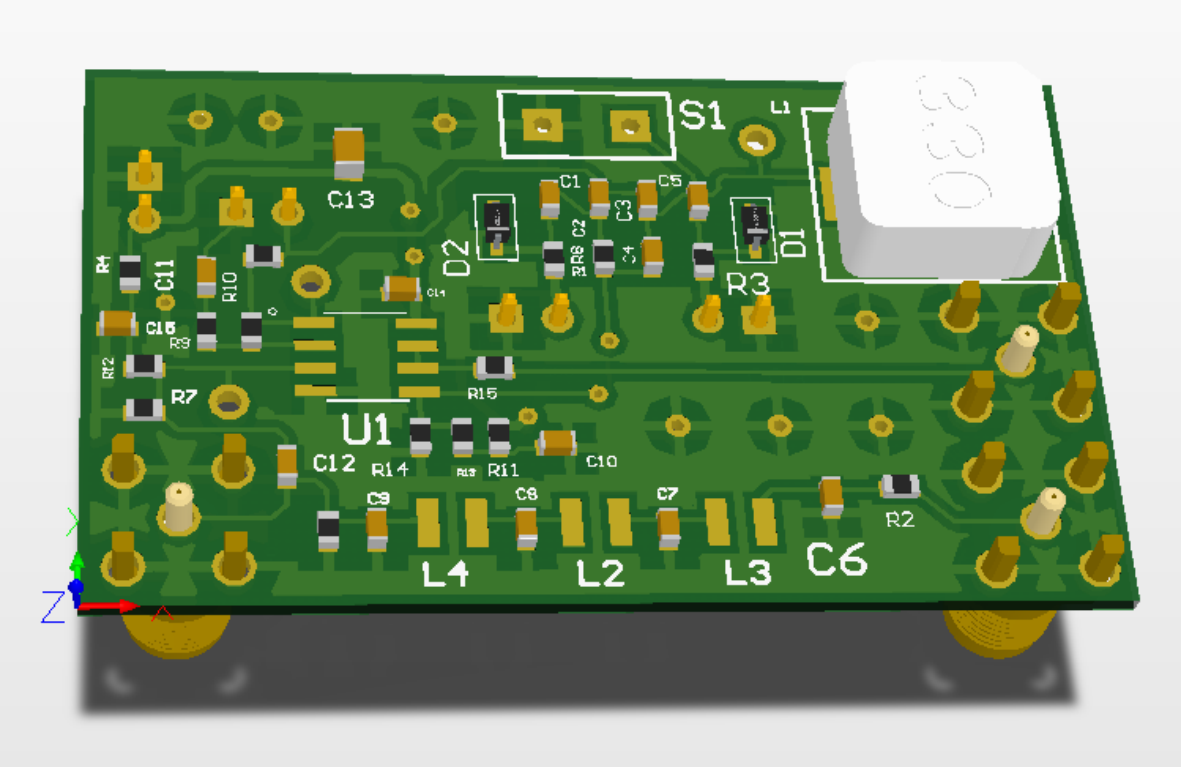

Figure A8: Sensor circuit prototype (top layer)

A.9. Sensor Circuit Prototype PCB (Bottom)

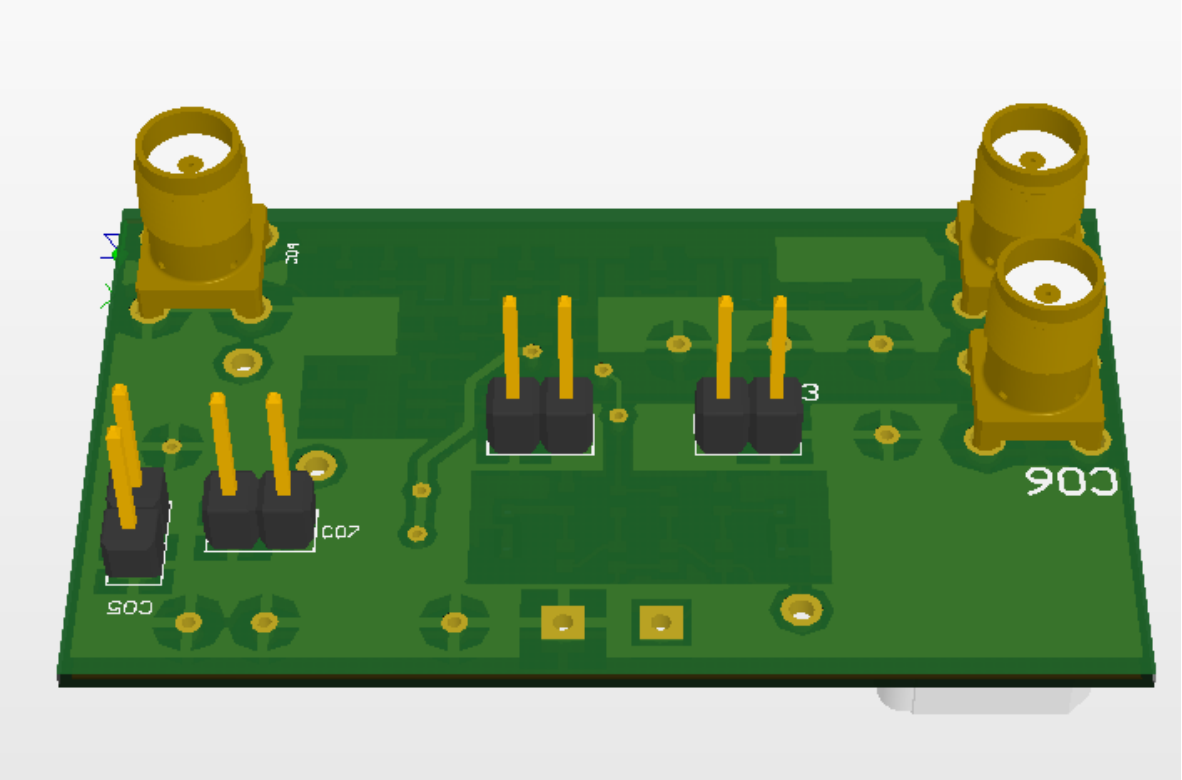

Figure A9: Sensor circuit prototype (bottom layer)

A.10. Amplifier Input and Output

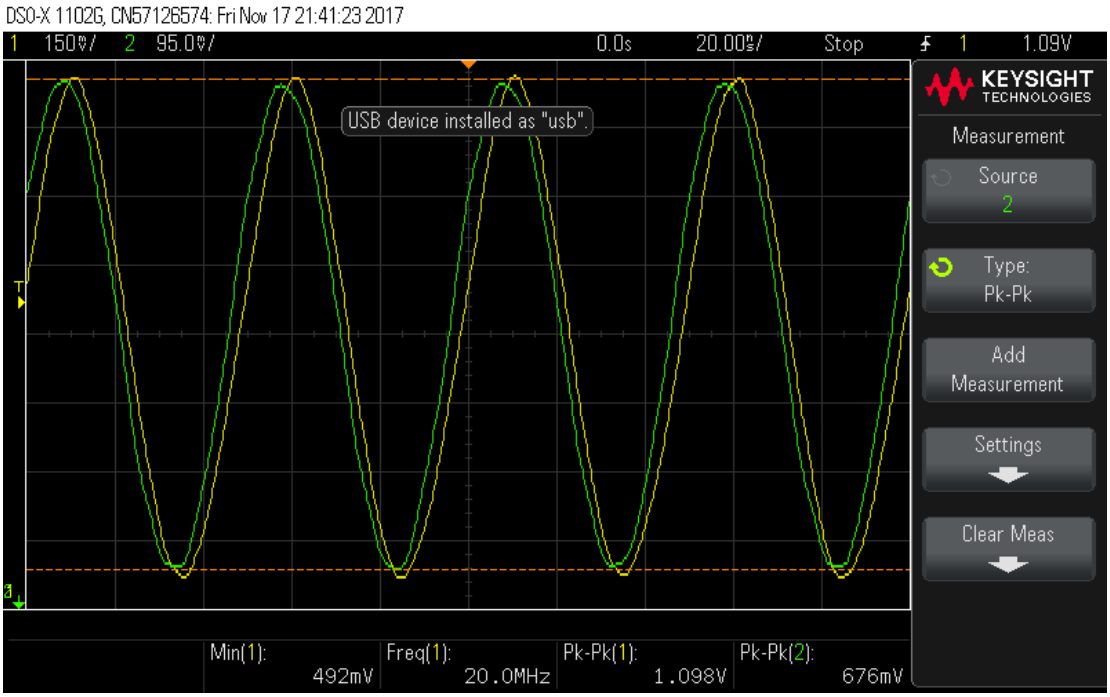

Figure A10: Full scale measurement of the amplifier signals

A.11. Squarewave Spectrum of the Agilent Signal Generator

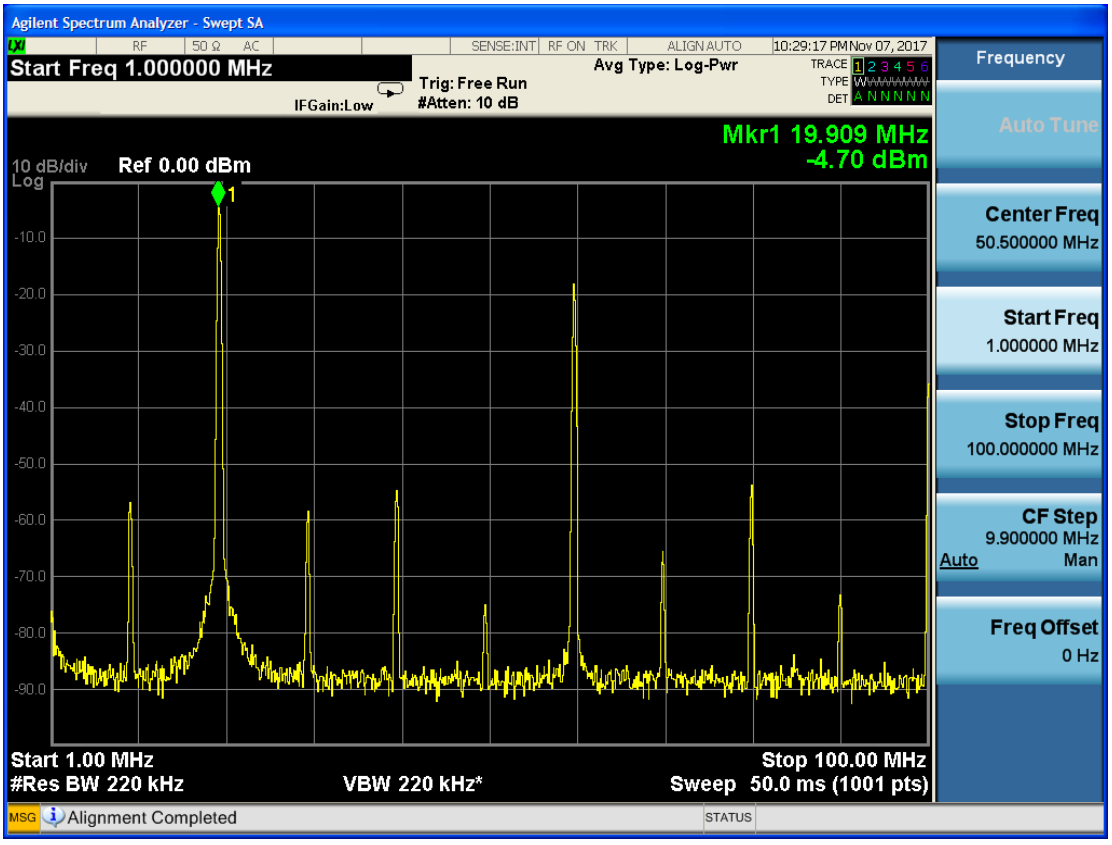

Figure A11: Spectrum of the 20Mhz square wave of the Agilent signal generator

A.12. Minimum Detection with Notch Prototype

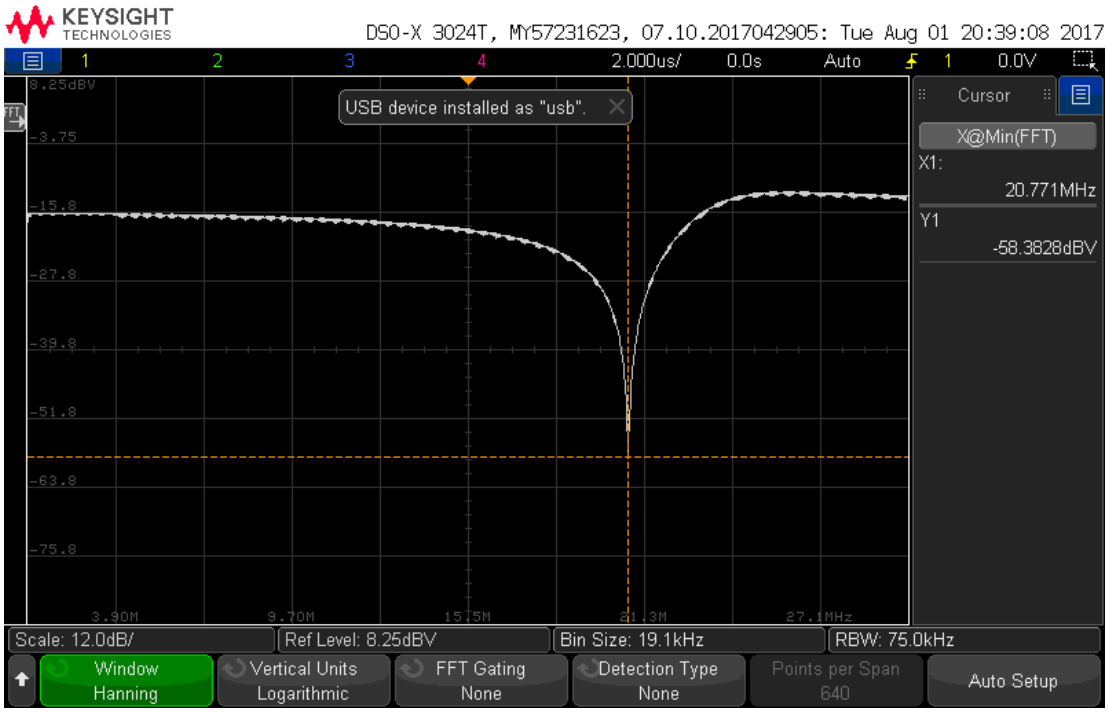

Figure A12: FFT, output voltage minimum at -60Db

A.13. Minimum Detection with Sensor Circuit Prototype

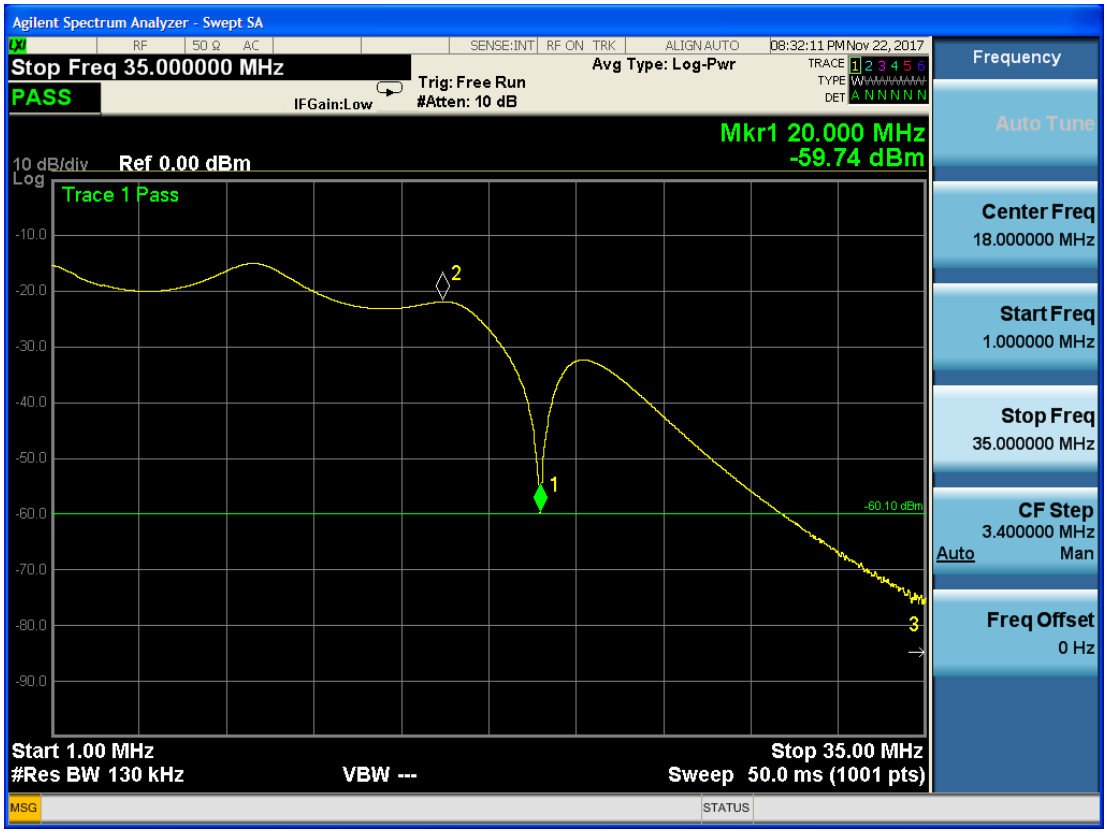

Figure A13: Calibration with air, minimum at -60dB @ 20MHz

A.14. Different Diode Capacitance Observations

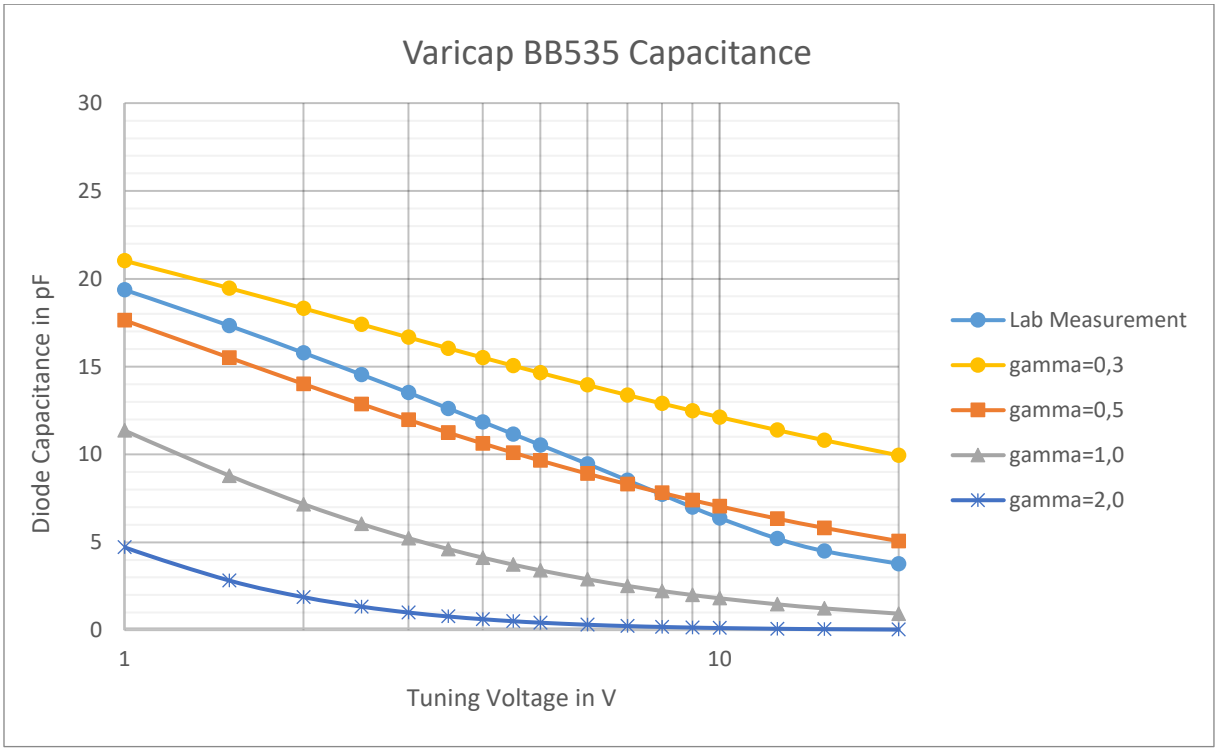

Figure A14: Diode Capacitance of BB535 with logarithmic x-axis

B. Supplementary Tables

B.1. Notch, BoM

Table B.1: Bill of materials, prototype notch

Component	Nominal Value	Manufacturer	Product
C1, C5	10nF	Murata	GRM39X7R104K16
C2, C3, C4	15pF	Murata	GRM39C0G150J50
R1, R3	100kΩ	TE Connectivity	CRG0603F100K
R2	200Ω	TE Connectivity	CRG0603F200R
L1	0,68µH	Bourns	SRR1050AR68Y
D1, D2	2,2pF-18,7pF	Infineon	BB535SOD323
CO1	1x4 Header	Molex	26604040

B.2. Sensor Circuit, BoM

Table B2: Bill of materials, sensor circuit prototype

Component	Nominal Value	Manufacturer	Product
C1, C5, C11, C12	10nF	Murata	GRM39X7R104K16
C2, C3, C4	15pF	Murata	GRM39C0G150J50
C6, C9	470pF	Murata	GRM39X7R471K50
C7, C8	680pF	Murata	GRM39X7R681K50
C10, C15	1nF	Murata	GRM39Y5V103Z50
C13	2,2uF		
C14	100nF	Murata	GRM39Y5V105Z10
R1, R3	100kΩ	TE Connectivity	CRG0603F100K
R8	200Ω	TE Connectivity	CRG0603F200R
R4, R7, R11, R12, R13, R14	10kΩ	TE Connectivity	CRG0603F10K
R2, R5, R15	0Ω	TE Connectivity	CRG0603ZR
R10	39Ω	TE Connectivity	CRG0603F39R
R6	1kΩ	TE Connectivity	CRG0603F1K0
R9	2kΩ	TE Connectivity	CRG0603F2K0
L1	0,68µH	Bourns	SRR1050AR68Y
L3, L4	330nH	Coilcraft	1008CS-331
L2	390nH	Coilcraft	1008CS-391
D1, D2	2,2pF-18,7pF	Infineon	BB535SOD323
U1		Texas Instruments	OPA2836ID
CO1, CO4, CO6	SMA Connector	Low Power Radio Solutions	SMA-RA-CONNECTOR
CO2, CO3, CO5, CO7	1x2 Header	RS Components	RS 670-5029

B.3. Output Frequency Measurement with the Prototype Notch

Table B3: Measurement table (figure 3.3)

ε'_R	f_{out}	Δf	V_{out}	V_{out}	Material
	in MHz	in kHz	in dBm	in mV	
1	20,00	0	-36,75	26,96	air
1,02	19,98	20	-36,45	27,43	dry sponge
2,26	19,74	260	-34,55	30,60	unknown type of plastic
4,01	19,56	440	-31,85	35,75	varnished wood

B.4. Diode Capacitance

Table B4.1: Diode Capacitance (BB535 datasheet vs. measurement – figure 2.6 and 2.7)

V_{Tuning}	$C_{Diode,\ Datasheet}$	V_{Tuning}	$C_{Diode,\ Measurement}$
in V	in pF	in V	in pF
1	18,7	0	27,37
2	15	0,01	27,23
5	9,5	0,1	26,05
10	5,3	0,2	24,92
15	3,35	0,4	23,07
20	2,61	0,5	22,31
25	2,24	0,75	20,68
28	2,1	1	19,37
		1,5	17,33
		2	15,78
		2,5	14,55
		3	13,52
		3,5	12,62
		4	11,85
		4,5	11,16
		5	10,54
		6	9,46
		7	8,53
		8	7,72
		9	7
		10	6,38
		12,5	5,21
		15	4,5
		20	3,78

Table B4.2: Diode Capacitance (BB535 datasheet – figure 2.7)

C_{Diode}	V_{Tuning}
in pF	**in V**
4	12,89
6	8,92
8	6,44
10	4,66
12	3,30
14	2,35
16	1,65
18	1,13

B.5. Output Amplitude Measurement with the Prototype Notch

Table 3.3: Measurement results of the effect of polarization losses on the output voltage

ε_R''	R_L	f_{out}	V_{out}	V_{out}	ΔV_{out}
$\cdot 10^{-3}$	**in kΩ**	**in MHz**	**in dBV**	**in mV**	**in mV**
0	0	19,999	-31,806	25,69	
10	36,170	20,003	-31,087	27,90	2,22
20	18,085	20,005	-30,430	30,10	4,41
30	12,057	20,007	-29,826	32,26	6,58
40	9,043	20,009	-29,261	34,43	8,74
50	7,234	20,013	-28,745	36,54	10,85
60	6,028	20,015	-28,259	38,64	12,95
70	5,167	20,015	-27,804	40,72	15,03
80	4,521	20,017	-27,375	42,78	17,09
90	4,019	20,019	-26,972	44,81	19,13
100	3,617	20,019	-26,590	46,83	21,14